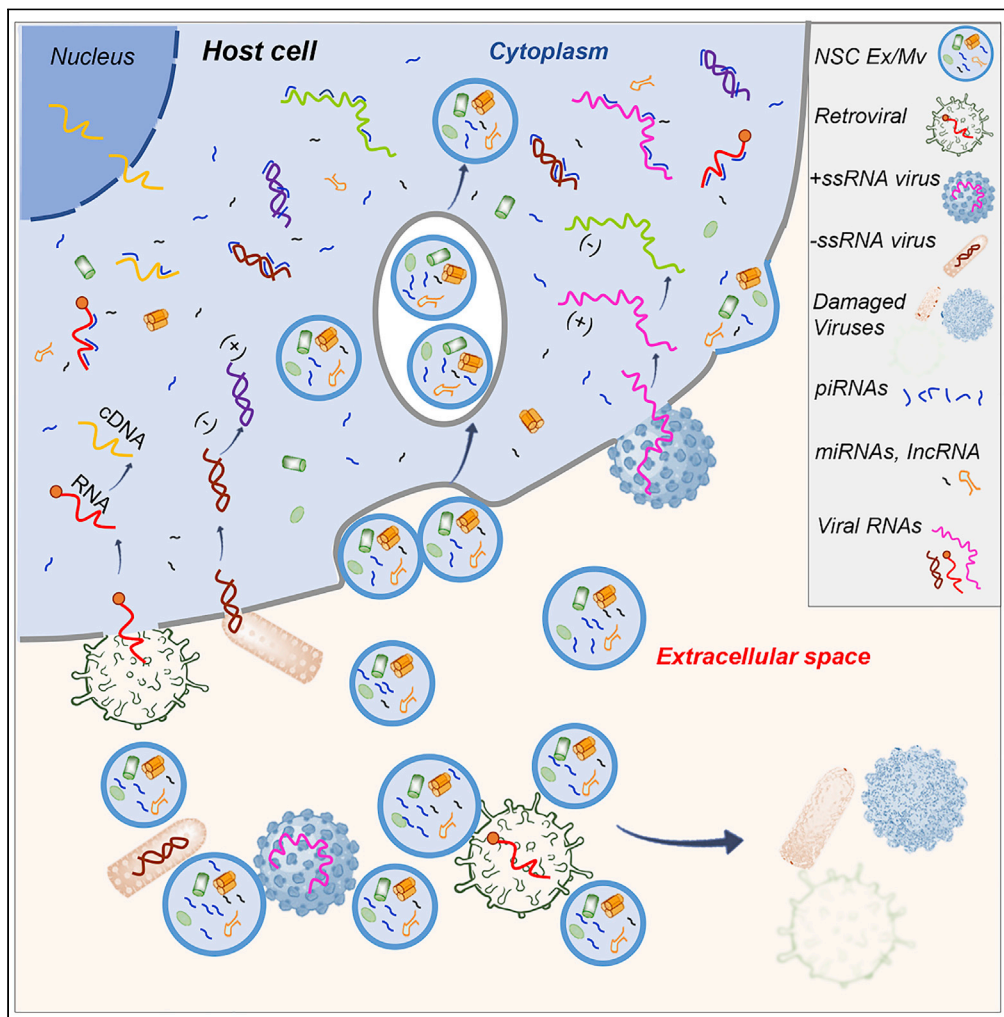


Article

# Innate and Adaptive Immunity of Murine Neural Stem Cell-Derived piRNA Exosomes/Microvesicles against Pseudotyped SARS-CoV-2 and HIV-Based Lentivirus



Bin Yu, Shoeb Ikhlas, Chunsheng Ruan, Xingxing Zhong, Dongsheng Cai

dongsheng.cai@einsteinmed.org

**HIGHLIGHTS**

Murine NSC-released exosomes/microvesicles have an innate antiviral action

Murine NSC-released exosomes/microvesicles can be induced adaptively to be antiviral

Murine NSC-released exosomes/microvesicles can target viruses in cell-free environment

Murine NSC exosomes/microvesicles produce piRNAs that are potentially antiviral

Yu et al., iScience 23, 101806  
December 18, 2020 © 2020  
The Author(s).  
<https://doi.org/10.1016/j.isci.2020.101806>



## Article

## Innate and Adaptive Immunity of Murine Neural Stem Cell-Derived piRNA Exosomes/Microvesicles against Pseudotyped SARS-CoV-2 and HIV-Based Lentivirus

Bin Yu,<sup>1</sup> Shoeb Ikhlas,<sup>1</sup> Chunsheng Ruan,<sup>1</sup> Xingxing Zhong,<sup>1</sup> and Dongsheng Cai<sup>1,2,\*</sup>

## SUMMARY

By testing pseudotyped SARS-CoV-2 and HIV-based lentivirus, this study reports that exosomes/microvesicles (Ex/Mv) isolated from murine hypothalamic neural stem/progenitor cells (htNSC) or subtype htNSC<sup>PGHM</sup> as well as hippocampal NSC have innate immunity-like actions against these RNA viruses. These extracellular vesicles also have a cell-free innate antiviral action by attacking and degrading viruses. We further generated the induced versions of Ex/Mv through prior viral exposure to NSCs and found that these induced Ex/Mv were stronger than basal Ex/Mv in reducing the infection of these viruses, suggesting the involvement of an adaptive immunity-like antiviral function. These NSC Ex/Mv were found to be characterized by producing large libraries of P element-induced wimpy testis (PIWI)-interacting RNAs (piRNAs) against genomes of various viruses, and some of these piRNAs were enriched during the adaptive immunity-like reaction, possibly contributing to the antiviral effects of these Ex/Mv. In conclusion, NSC Ex/Mv have antiviral immunity and could potentially be developed to combat against various viruses.

## INTRODUCTION

The brain is the “headquarters” of the body and normally should be strictly protected from infections especially by viruses, which are small and could penetrate into the brain parenchyma with less difficulty than large pathogens such as bacteria. This antiviral protection theoretically requires brain immunity, but it is much less clear how the brain fights against viral infection compared with the immune operation in the periphery. Recently, as research has appreciated the neural control of immunity (Pavlov et al., 2018; Rosas-Balina et al., 2011; Wang et al., 2020), some evidence was obtained to help understand brain immunity; for instance, the brain has the lymphatic system (Da Mesquita et al., 2018; Louveau et al., 2015; Moseman et al., 2020; Papadopoulos et al., 2020) and olfactory stem cells have an immune defense effect under chronic inflammation (Chen et al., 2019). Related to this research field, we discovered that the hypothalamus has a role in linking innate immunity to adaptive immunity (Kim et al., 2015) and hypothalamic neural stem/progenitor cells (htNSC) abundantly secrete exosomal microRNAs (miRNAs) into the cerebrospinal fluid while some of these miRNAs target immunity components (Zhang et al., 2017). Here in this study, we report that murine NSCs produce exosomes/microvesicles (Ex/Mv) to provide innate and adaptive antiviral actions, using recombinant viruses as examples. Furthermore, we found that these NSC Ex/Mv are characterized by producing large libraries of P element-induced wimpy testis (PIWI)-interacting RNAs (piRNAs) against the genomes of various viruses, and some of these piRNAs can be further enriched in the induced versions of NSC Ex/Mv, likely contributing to the antiviral effects of these vesicular particles. All these findings suggest a value of developing NSC-derived piRNAs-containing Ex/Mv for combating against various viruses, possibly including SARS-CoV-2.

## RESULTS

## Innate Antiviral Immunity of Murine NSC Ex/Mv against Pseudotyped SARS-CoV-2

Glycoprotein-deficient vesicular stomatitis virus ( $\Delta$ G-VSV) is a standard tool to create pseudotyped viruses (Whitt, 2010), and it has frequently been used to generate pseudotyped viruses and the recently

<sup>1</sup>Department of Molecular Pharmacology, Albert Einstein College of Medicine, 1300 Morris Park Avenue, Bronx, NY 10461, USA

<sup>2</sup>Lead Contact

\*Correspondence: dongsheng.cai@einsteinmed.org

<https://doi.org/10.1016/j.isci.2020.101806>



pseudotyped SARS-CoV-2 virus (Nie et al., 2020). Because ΔG-VSV was designed to accurately report viral infection, we incorporated wild-type SARS-CoV-2 spike protein into luciferase-expressing ΔG-VSV to generate a pseudotyped SARS-CoV-2 virus. The infection of host cells by this virus was quantitatively reflected by measuring the activity of luciferase, which was encoded by this viral genome. We employed this pseudotyped SARS-CoV-2 to study if murine NSC-released extracellular vesicles might have an action to fight against this virus. As we previously revealed (Zhang et al., 2017), murine NSC abundantly produce and release exosomes, which are extracellular vesicles of small size (usually below 200 nm in diameter); this study was based on these exosomes, and also included microvesicles (together referred to as Ex/Mv), the latter are the extracellular vesicles of large size (usually above 200 nm in diameter). We designed to comparatively study Ex/Mv from NSCs including htNSC, hpNSC, as well as htNSC<sup>PGHM</sup>, an htNSC subtype that we recently established, because Ex/Mv from this htNSC subtype can importantly help animals survive from fatal conditions besides the benefit that this NSC subtype can be applied peripherally (Tang et al., 2020). To do so, we isolated and purified Ex/Mv that were released from these NSCs in culture and then tested if treatment with these Ex/Mv could provide a therapeutic effect against the infection of these pseudotyped SARS-CoV-2 viruses *in vitro*. To mimic its infection in various organs, we employed two human respiratory cell models, human alveolar basal epithelial cell A549 and human bronchial epithelial cell Calu3, and human hepatocyte cell model HepG2, all of which express human angiotensin-converting enzyme 2 (hACE2) and have been used to study SARS-CoV-2 recently (Hoffmann et al., 2020; Ma et al., 2020; Nie et al., 2020). We infected these cells with pseudotyped SARS-CoV-2 and in the meanwhile treated these cells with Ex/Mv derived from an NSC type versus vehicle control. The results showed that treatment of NSC Ex/Mv regardless of NSC types provided a significant antiviral effect in A549 and HepG2 cells (Figures 1A and 1B). However, infection in Calu3 cells was not affected by this treatment (Figure 1C), suggesting that some cells are less sensitive than others in responding to the treatment. We further verified these antiviral effects in A549 and HepG2 cells through immunostaining of luciferase protein. As represented in Figure 1D and quantified in detail in Figure 1E, whereas luciferase protein was strongly present in cells with vehicle control group, it was only weakly present in cells that were treated with either type of NSC Ex/Mv. Hence, NSC Ex/Mv have innate antiviral actions for some human cells of different tissue origins.

### Adaptive Antiviral Immunity of Murine NSC Ex/Mv against Pseudotyped SARS-CoV-2

We noted that compared with A549 and HepG2, Calu3 cells were not responsive to the treatment of NSC Ex/Mv (Figure 1C), and thus wondered if these NSC Ex/Mv could be optimized for an antiviral effect for targeting insensitive cells such as Calu3. We asked if an initial exposure of a specific virus to NSC could lead to an enhancement or enrichment of certain immunity features of NSC-derived Ex/Mv, which could boost the antiviral actions. Because infection of pseudotyped SARS-CoV-2 requires hACE2 as the receptor, we generated hACE2-NSC cell lines with overexpression of hACE2 through the process of lentiviral induction and selection (Figure 2A). After these cell lines were stably maintained for several generations in culture, we treated these cells with the pseudotyped SARS-CoV-2 for two generations and then maintained them under normal culture for about five generations. After that, we isolated and purified Ex/Mv from these virally pre-exposed NSCs versus matched basal NSCs, leading to the generation of induced versus basal versions of NSC Ex/Mv, respectively. As infection of Calu3 cells was insensitive to basal NSC Ex/Mv treatment, this cell line represented a unique experimental model for comparing the effects of induced versus basal Ex/Mv. As shown in Figure 2B, whereas basal NSC Ex/Mv were ineffective, we excitingly found that the induced NSC Ex/Mv, regardless of NSC types, became consistently effective in reducing the infection of pseudotyped SARS-CoV-2 in Calu3 cells. Thus, NSC Ex/Mv can be induced via an adaptive immunity-like process to provide improved effects against viral infection.

### A Cell-Independent Antiviral Action of NSC Ex/Mv against Pseudotyped SARS-CoV-2

Ex/Mv and RNA viruses are similarly small-sized membranous particles, and both consist of RNA sequences. We were provoked to question if NSC Ex/Mv might have an innate immunity-like action to directly interact with viruses in a cell-free environment. To answer this question, we incubated NSC Ex/Mv with pseudotyped SARS-CoV-2 and then examined how this incubation could affect the virus. To test this idea directly, we employed transmission electron microscopy (TEM) to observe if there could be any physical interaction between NSC Ex/Mv and viruses. In this experiment, we designed to focus on exosomes (below 200 nm in diameter) from htNSC Ex/Mv, which were isolated through a filter. We then mixed these htNSC-derived exosomes with pseudotyped SARS-CoV-2 in a buffer for 0.5 h at room temperature and then overnight at 4°C before fixing and processing with negative staining for TEM analysis. Exosomes or viruses alone in the same reaction condition were included to provide technical controls. Clearly, exosomes

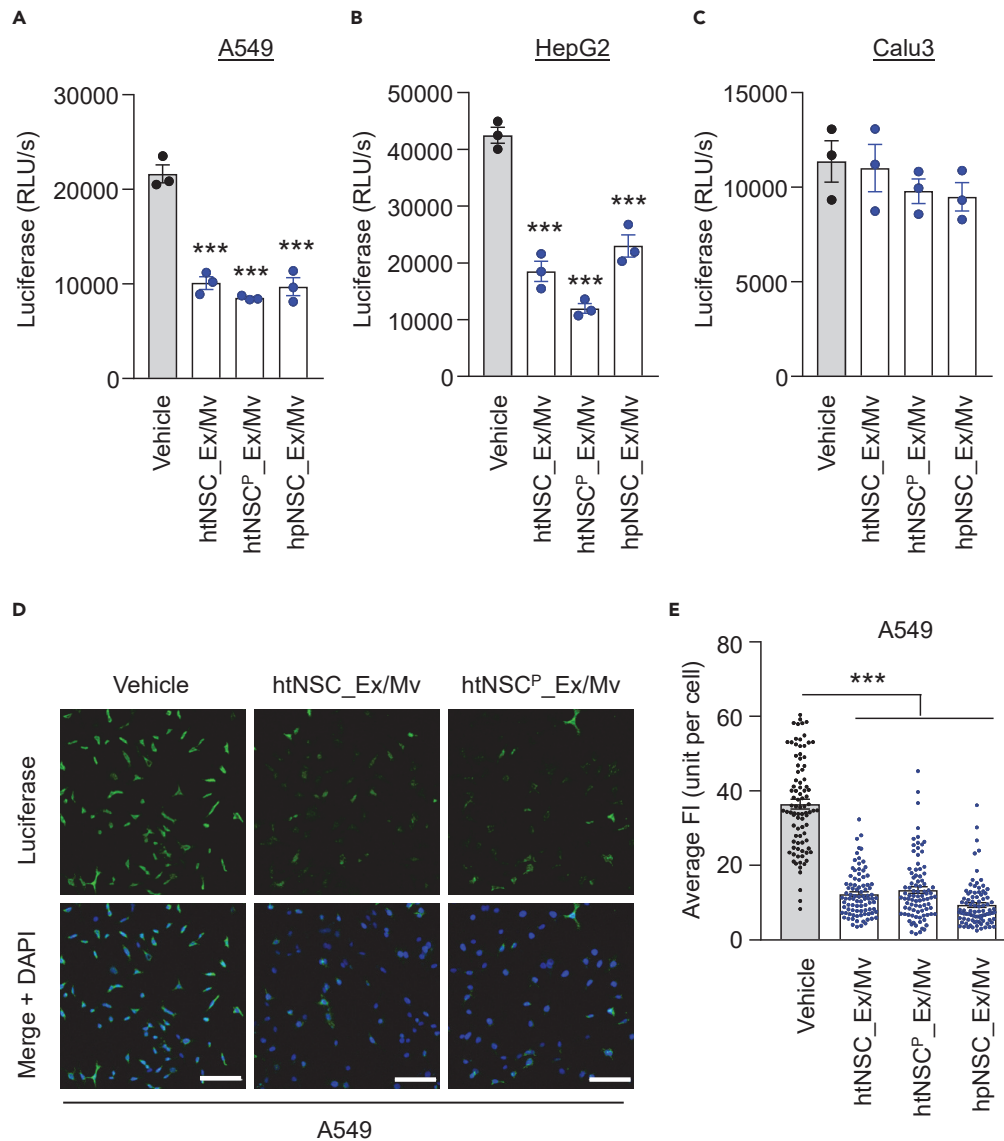


**Figure 1. Innate Antiviral Effects of NSC Ex/Mv against Pseudotyped SARS-CoV-2**

(A–E) Cultured A549, HepG2, and Calu3 cells were infected with pseudotyped SARS-CoV-2 (wild-type SARS-CoV-2 spike protein-incorporated  $\Delta$ G-luc-VSV) in the presence or absence of purified Ex/Mv that were isolated from indicated NSC types, and 24 h later these cells were harvested for the measurement of luciferase activities (A–C) or fixed for immunostaining of luciferase (D and E). Immunostaining images presented were based on htNSC Ex/Mv and htNSC<sup>P</sup> Ex/Mv treatment, whereas images of all NSC groups were quantitatively analyzed in right panels (randomized 90 cells per group were analyzed, each dot represented the average fluorescence intensity [FI] of a single cell). htNSC<sup>P</sup>: htNSC<sup>PGHM</sup>. Scale bars, 100  $\mu$ m. \*\*\* $p < 0.001$ ; ANOVA/post-hoc, compared between indicated groups,  $n = 3$  independent biological samples per group, values represent the mean  $\pm$  SEM.

and viruses had distinctly different morphologies, as viruses were rod-shaped, whereas exosomes were round and cup-shaped. We observed that whereas typically viruses and exosomes were both spreadingly and randomly distributed in the TEM fields, mixture with NSC exosomes led to clustered aggregations and ring-like structures (Figure 3A). Through high-magnification TEM imaging, we identified morphological evidence suggesting that exosomes physically attached, surrounded, or engulfed viruses, and some of these behaviors were apparently associated with breakdown and degradation of viruses (Figure 3B). Independently, we performed experiments in which pseudotyped SARS-CoV-2 viruses were mixed with NSC Ex/Mv versus vehicle in a buffer and then subjected to western blotting for SARS-CoV-2 spike

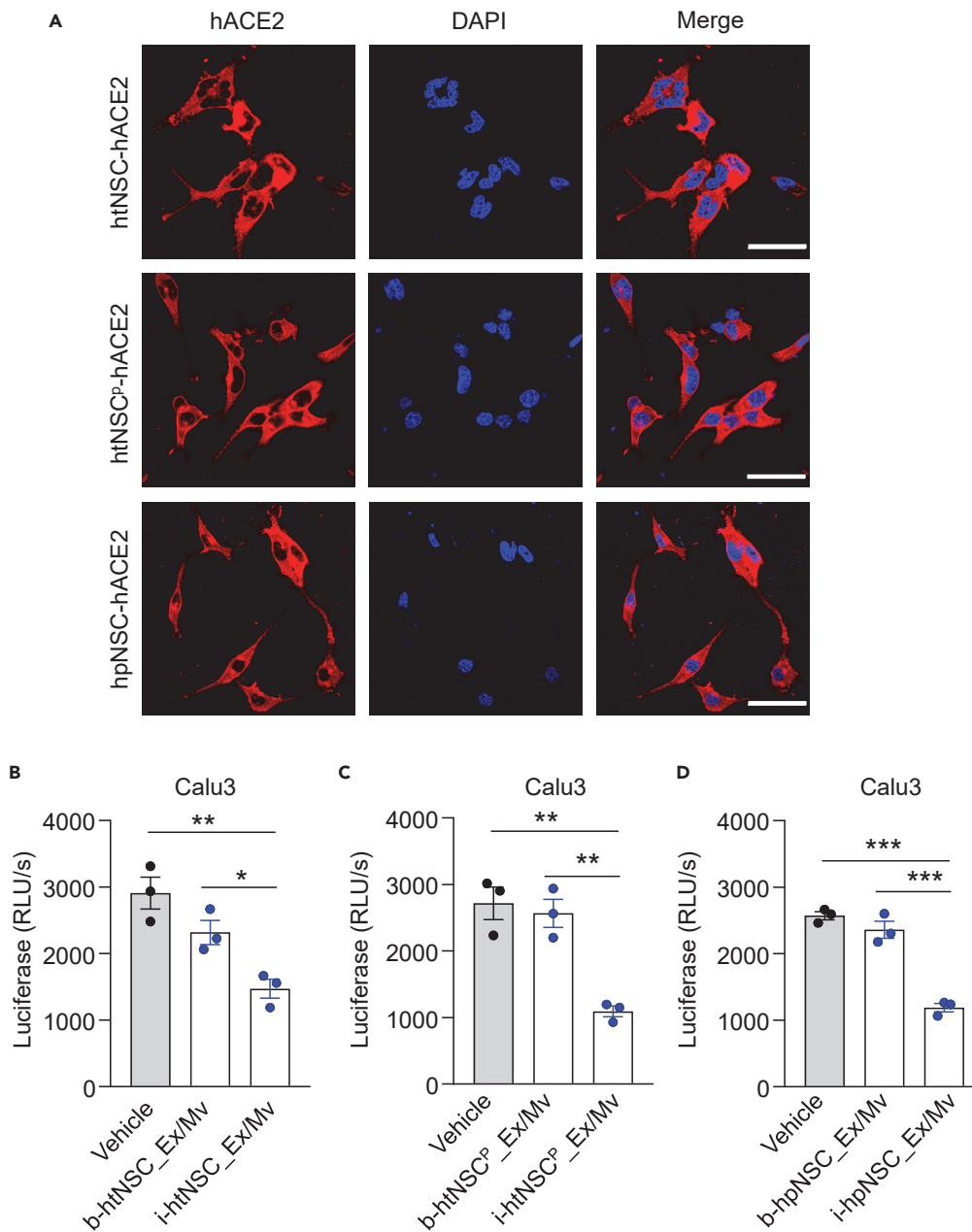


**Figure 2. Adaptive Antiviral Effects of NSC Ex/Mv against Pseudotyped SARS-CoV-2**

(A) Types of NSCs as indicated were induced with hACE2-expressing lentivirus (controlled by CMV promoter) and selected through the antibiotics to make stable cell lines. These cells were evaluated through immunostaining via hACE2 antibody. DAPI staining was included to show cell nuclei. htNSC<sup>P</sup>: htNSC<sup>P</sup>. Scale bars, 50  $\mu$ m.

(B–D) Cultured Calu3 cells were infected with pseudotyped SARS-CoV-2 in the presence or absence of purified Ex/Mv from a basal (labeled as “b-”) or induced (labeled as “i-”) NSC types including htNSC (B), htNSC<sup>P</sup> (C) and hpNSC (D) versus vehicle (B–D), and 24 h later these cells were harvested for the measurement of luciferase activities. htNSC<sup>P</sup>: htNSC<sup>P</sup>. \* $p < 0.05$ , \*\* $p < 0.01$ , \*\*\* $p < 0.001$ ; ANOVA/post-hoc, compared between indicated groups,  $n = 3$  independent biological samples per group, values represent the mean  $\pm$  SEM.

protein. The results showed that the mixture with htNSC or hpNSC Ex/Mv both led to degradation of this spike glycoprotein (Figure 4A). Furthermore, we performed an experiment in which pseudotyped SARS-CoV-2 and NSC Ex/Mv were maintained separately or were mixed together for an overnight period and then were used to infect HepG2 cells. As shown in Figure 4B, pre-mixture of these viruses with either

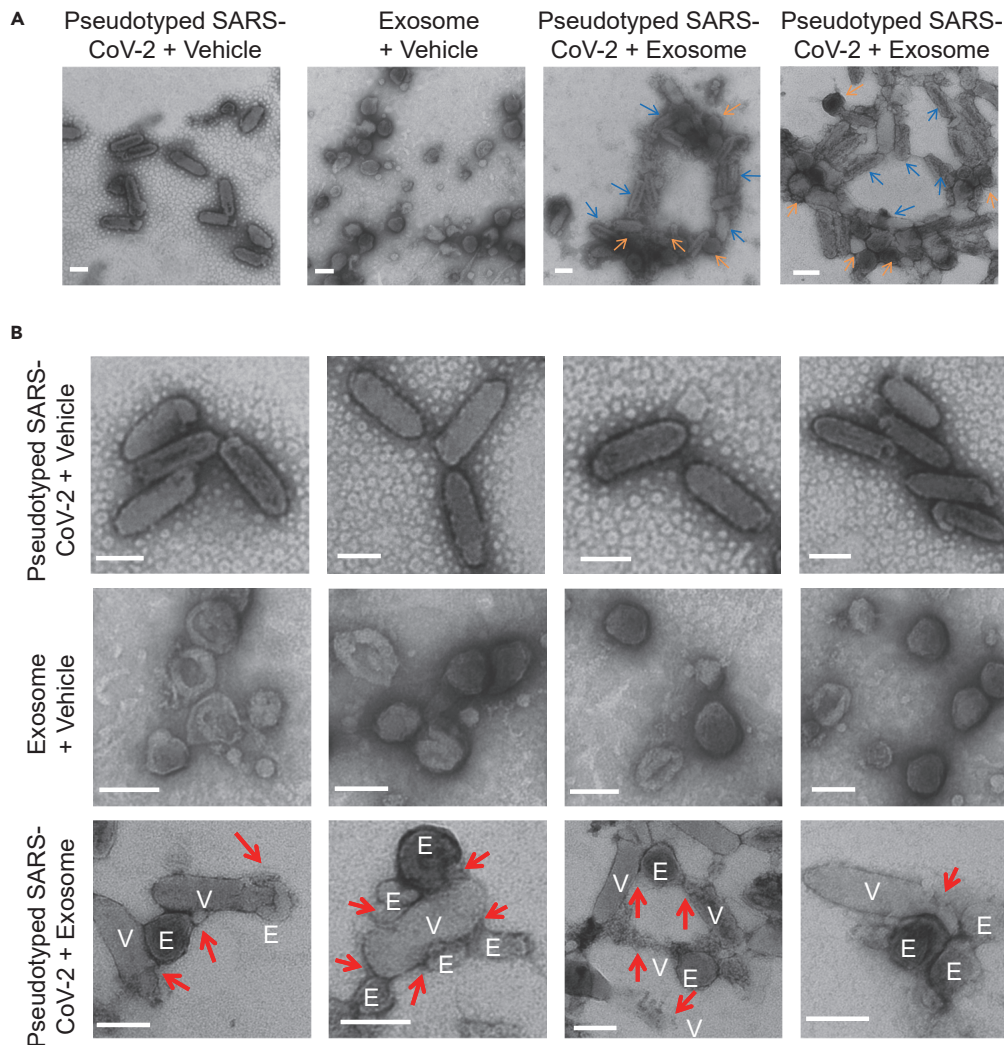


**Figure 3. Physical Interactions of NSC Exosomes with Pseudotyped SARS-CoV-2**

Pseudotyped SARS-CoV-2 (SARS-CoV-2 spike protein-enveloped  $\Delta$ G-luc-VSV) were mixed with purified htNSC exosomes (without including microvesicles) versus vehicle control and incubated for 0.5 h at room temperature and then overnight at 4°C.

(A and B) Samples were employed to perform uranyl acetate negative staining and TEM on grids and examined at regular (A) and high (B) magnification. E: exosome, V: virus. The blue arrows point to virus and the orange arrows point to exosome (A), whereas the red arrows point to exosome-virus interaction or damaged virus (B). Images are presented repeatedly from two areas of TEM imaging for “pseudotyped SARS-CoV-2 + exosome” (A) and repeatedly from four areas of TEM imaging for each group (B). Scale bars, 100  $\mu$ m.

type of NSC Ex/Mv led to an evident reduction in the abilities of these viruses to infect the host cells. Altogether, these results suggest that NSC Ex/Mv have a cell-independent innate antiviral effect in cell-free environment.

### Antiviral NSC Ex/Mv Are Characterized by Containing piRNA Machinery

We have previously revealed that murine NSCs abundantly produce exosomal miRNAs (Zhang et al., 2017). Because miRNAs are known to target mainly mRNAs, we directed our attention to piRNAs, a different type of small RNAs that can target many other types of RNA/DNA, and there are huge numbers of piRNA species in various animals including rodents (Wang et al., 2019), although research often focuses on germ cells for piRNA biology since the discovery. The activities of piRNAs are mediated by PIWI proteins, mainly PIWI1 and PIWI2 (PIWIL1 and PIWIL2 in mammals, respectively). We decided to employ PIWIL1/2 as the

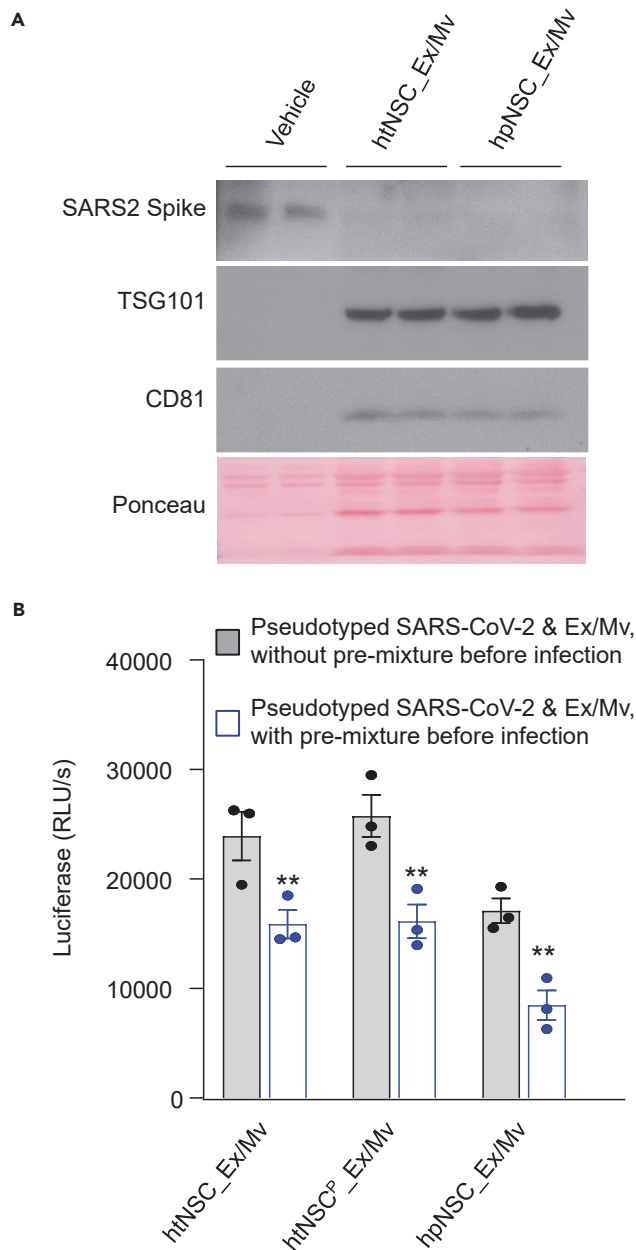


**Figure 4. Cell-Free Antiviral Effects of NSC Ex/Mv against Pseudotyped SARS-CoV-2**

(A) Pseudotyped SARS-CoV-2 were mixed with indicated Ex/Mv versus vehicle and incubated for 0.5 h at room temperature and then overnight at 4°C. Samples were then lysed and processed for western blot using antibodies against SARS-CoV-2 spike protein (labeled as SARS2 Spike) or Ex/Mv markers CD81 and TSG101. Ponceau staining of the gels provided a technical control.

(B) Pseudotyped SARS-CoV-2 (SARS-CoV-2 spike protein-enveloped ΔG-luc-VSV) and indicated NSC Ex/Mv were maintained separately (labeled as “without pre-mixture”) or mixed together (labeled as “with pre-mixture”) for an overnight period (0.5 h at room temperature followed by 4°C) and these Ex/Mv and viruses with vs. without pre-mixture were then used to treat HepG2 cells for 24 h. Subsequently these cells were harvested and lysed for measurement of luciferase activities. \*\*p < 0.01; ANOVA/post-hoc, compared between indicated groups, n = 3 independent biological samples per group, values represent the mean ± SEM.

biomarkers to analyze if the piRNA machinery could be contained in NSC Ex/Mv, which we have found antiviral. First, we examined if PIWIL1/2 proteins could be detectable in NSCs at the cellular level, and for comparison, we included mesenchymal stem cells (MSC) in this experimental assay. PIWIL1 blot did not yield clear signals in western blots, whereas we found that PIWIL2 was evidently expressed in htNSC and htNSC<sup>PGHM</sup> as well as hpNSC, but comparatively its expression level was much lower in MSC (Figure 5A). In parallel, we employed PIWIL2 immunostaining to compare the cellular distribution of this protein in NSC and MSC. We found that PIWIL2 was present mainly in the nuclei of MSC; in contrast, PIWIL2 was present strongly in the cytoplasm of all NSC types in addition to the nuclear distribution of this protein (Figure 5B). The cytoplasmic distribution of PIWI protein is theoretically consistent with the source of this protein for piRNA machinery in NSC Ex/Mv. In this context, we directly examined PIWIL2 in antiviral NSC Ex/Mv focusing on exosomes through immunostaining and imaging under high magnifications. As represented in Figure 5C, we consistently confirmed that these NSC-derived exosomes contained PIWIL2. Under co-staining condition, the immunostaining signals of PIWIL2 were comparable to the levels as revealed by exosomal markers TSG101 and CD81, suggesting that PIWIL2 in these vesicles was significant. Hence, NSC Ex/Mv were characterized by containing piRNA machinery while being antiviral.

### NSC Ex/Mv Contain piRNA Libraries Potentially against SARS-CoV-2 Genome

Thus, we searched for mouse piRNAs that could match against the genomic RNA sequence of SARS-CoV-2 virus including the encoding sequences for spike protein; envelope protein; membrane protein; nucleocapsid protein; open reading frame (Orf) sequences Orf1ab, 3a, 6, 7a, 7b, 8, and 10; UTR sequences at the 5' and 3' ends; and three gap structural sequences (gap 1–3), as elucidated in Figure S1A. Although SARS-CoV-2 is single-strand RNA virus, we analyzed both sense and antisense sequences because production and replication of RNA viruses in host cells involve the synthesis of both strands. A piRNA has the primary lead sequence made of nucleotides from positions 2 to 11 and the secondary lead sequence made of nucleotides from positions 12 to 21; although the targeting rules of piRNAs in mammals are still not clearly established, it has recently been described in *C. elegans* that matching of primary lead and particularly nucleotides 2–8 with target RNA is important; the secondary lead sequence could have a few mismatches with target RNA (Shen et al., 2018; Zhang et al., 2018). To begin with, we screened for piRNAs that have at least 16 nucleotides matching with SARS-CoV-2 RNA and found over thousand unique piRNA species that met this requirement; diagram in Figure S1A presented a portion of these piRNAs with sequence information detailed in Table S1. For piRNAs in this table, we further required perfect match of the primary lead nucleotides 2–11 and no more than four mismatches for the secondary lead nucleotides 12–21 (Criteria #1) and found that about 170 piRNA species met these criteria (Figure S1A, Table S1). Given that SARS-CoV-2 viruses have many variants and mutations, we slightly adjusted the criteria by allowing five mismatches in the secondary lead sequence, whereas the primary lead sequence was still required for perfect matches (Criteria #2). This led to identification of ~150 additional piRNA species that could target SARS-CoV-2 (Figure S2A, Table S1). Hence, mouse species has piRNAs against sense and antisense sequence of SARS-CoV-2 genome. It should be mentioned that this analysis was based on piRNAQuest, a database which is not a complete collection of piRNAs. We also did the same way for human piRNAs through this database but noted that there are much fewer human piRNA species meeting these criteria of targeting SARS-CoV-2. If this difference is verified through complete analysis of additional piRNA databases, it might point to the importance of piRNAs for the different resistance to viral infection between rodents and humans.

We then quantitatively measured some of these piRNAs in NSC Ex/Mv. To do so, we studied Ex/Mv from NSC compared with Ex/Mv from MSC. We randomly examined about 60 piRNA species that could target different regions of this genome based on Criteria 1 or 2. The results showed that most of these piRNAs were clearly present in NSC Ex/Mv (using htNSC<sup>PGHM</sup> and hpNSC as the representative); in contrast, these piRNAs were much less detectable in MSC Ex/Mv. Relatively, the levels of some piRNAs were 100- to 30,000-fold higher in NSC Ex/Mv than in MSC Ex/Mv, based on the same quantity of Ex/Mv total small RNA (Figure S1B). In addition, we confirmed that these piRNAs were similar or slightly higher in htNSC<sup>PGHM</sup> Ex/Mv when compared with the levels in htNSC Ex/Mv; thus, as a subtype of htNSC, htNSC<sup>PGHM</sup> capture the feature of NSCs in producing Ex/Mv piRNAs. On the other hand, we noted in several cases that the cellular levels of piRNAs were relatively comparable between NSC and MSC, which can, however, further point to the special feature of NSC for actively assembling piRNAs into the secretory Ex/Mv of these neural cells.

### NSC Ex/Mv piRNAs against Pseudotyped SARS-CoV-2 and Their Adaptive Enrichment

The genome of the pseudotyped SARS-CoV-2 in this study was based on VSV elements, including the RNA sequences encoding nucleocapsid protein (N sequence), phosphoprotein (P sequence), matrix



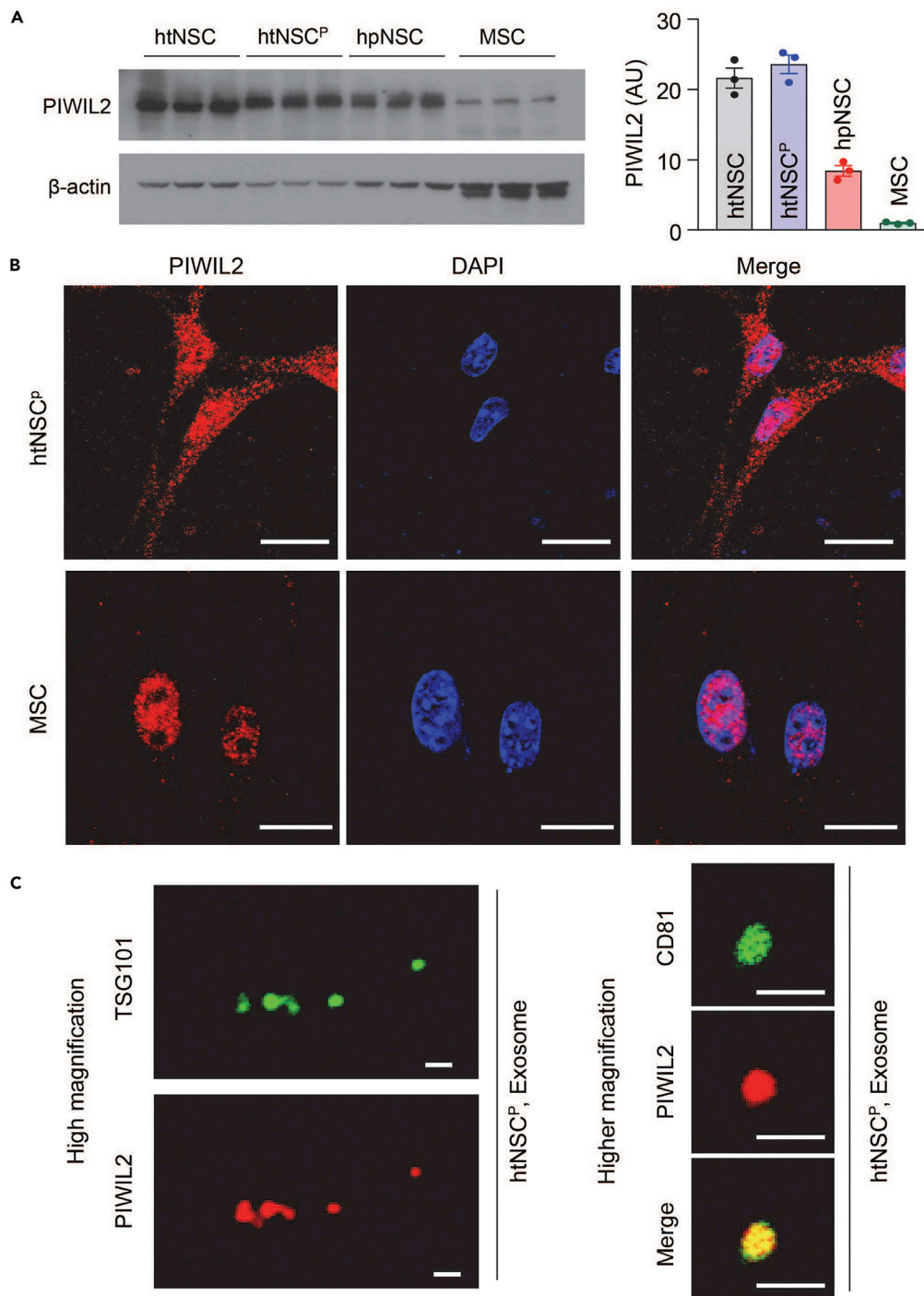


**Figure 5. PIWIL2 Machinery in NSC and NSC-Secreted Ex/Mv**

(A) Western blot of PIWIL2 in Ex/Mv isolated from mouse htNSC, htNSC<sup>PGHM</sup> (labeled as htNSC<sup>P</sup>), hpNSC, and MSC.  $\beta$ -Actin blot of the same membrane was included as a reference. Right panel shows quantification of PIWIL2 expression levels normalized by  $\beta$ -actin expression levels in each cell type. AU: arbitrary unit.

(B) Immunostaining of PIWIL2 (red) for cultured NSCs and MSC. The panel shows the images of htNSC<sup>P</sup> (representing other NSCs) and MSC. DAPI nuclear staining (blue) was included as a reference. Scale bars, 20  $\mu$ m.

(C) Co-immunostaining of PIWIL2 (red) and exosomal marker TSG101 (green) or CD81 (green) for Ex/Mv focusing on exosomes released from cultured htNSC<sup>P</sup> (representing other NSCs). Left panel shows a representative high-magnification view of individual exosomes. Right panel shows a representative higher-magnification view of single exosome particle. Scale bars, 500 nm.

protein (M sequence), RNA polymerase (R sequence), and structural non-encoding sequences (S1-6), as elucidated in [Figure S2A](#). We applied each of these sense and antisense sequences to screen for piRNA species through mouse piRNAQuest database and found a long list of piRNAs with at least 15–16 nucleotides matching with the viral sequence, and among them, about 40 piRNA species were identified to meet Criteria 1 or 2 ([Figure S2A](#), [Table S2](#)). We then measured some of these piRNAs in NSC Ex/Mv (using htNSC<sup>PGHM</sup> and hpNSC as the representative) compared with the levels in MSC Ex/Mv. As shown in [Figures S2B](#) and [S3](#), most of these piRNAs were present in these NSC Ex/Mv but were much less detectable in MSC Ex/Mv. Our additional assays showed that htNSC<sup>PGHM</sup> were comparable or slightly stronger than htNSC in producing these piRNAs. Thus, based on the information from wild-type and pseudotyped SARS-CoV-2, NSC Ex/Mv contain piRNAs against the genomic sequences of both viruses, although these NSC were not previously exposed to either virus, suggesting that mouse species has evolved to establish large antiviral piRNA libraries in NSC Ex/Mv.

We asked if an initial pre-exposure of a specific virus to NSC could lead to an enhancement or enrichment of specific antiviral piRNAs in NSC Ex/Mv. Thus, we treated these NSCs with pseudotyped SARS-CoV-2 virus for two generations, and then maintained them under normal culture for about five generations. After that, we isolated and purified Ex/Mv from these virally pre-exposed NSCs versus matched basal NSCs and then measured their piRNA expression levels via qPCR. Among about 80 piRNAs that we examined, roughly half were significantly upregulated due to the viral pre-exposure, typically 5- to 10-fold higher than the basal levels ([Figure S4](#)). Of note, the increased expression levels in these specific piRNAs were often due to relative downregulation in non-target small RNAs (such as U6 miRNA as an example) in these induced Ex/Mv compared with basal Ex/Mv, suggesting that at least a negative selection process occurred. We also evaluated this effect based on luciferase-encoding sequence in this viral genome, because we found a short list of piRNA species, which even matched against the sense or antisense sequence of luciferase RNA ([Table S2](#)), although luciferase is a non-viral protein. We measured seven of these piRNA species and found that five of them were present in NSC Ex/Mv but much less detectable in MSC Ex/Mv ([Figure S5A](#)), indicating that murine NSC Ex/Mv have piRNA libraries against various types of foreign genomic sequences, which are not limited to viral genomes. We examined if these piRNAs could be upregulated by viral pre-exposure and found that four of them showed significant upregulation ([Figures S5B](#) and [S5C](#)). Thus, viral genome-specific piRNAs in NSC Ex/Mv can be enriched and enhanced in response to viral pre-exposure to possibly contribute to the better antiviral effect of these vesicles against this particular virus.

### Innate and Adaptive Antiviral Actions of NSC Ex/Mv against HIV-Based Lentivirus

To further assess the predicted antiviral role of murine NSC Ex/Mv, we extended the study to examine an RNA virus unrelated to SARS-CoV-2, i.e., HIV-based lentivirus. This viral model was based on a VSV glycoprotein (VSVG)-enveloped recombinant lentivirus, and it also expressed GFP (controlled by CMV promoter) when host cells are infected. We examined if treatment with NSC Ex/Mv could provide a protective effect against lentiviral infection in A549 cells. For comparison, we generated the same amount of Ex/Mv from MSC for the treatment. As shown in [Figure 6A](#), the number of GFP-positive cells due to lentiviral infection was clearly reduced by the treatment of NSC Ex/Mv, whereas treatment with MSC Ex/Mv did not have such an effect. Then, we further quantitatively analyzed this antiviral therapeutic effect of NSC Ex/Mv treatment via western blotting. Our western blot for lentiviral GFP revealed that this treatment with NSC Ex/Mv led to a reduction in lentiviral infection ([Figure 6B](#)). Subsequently, we compared the basal and induced NSC Ex/Mv for the antiviral effects in A549 cells. To better discern the difference between induced and basal versions, we employed a stronger infection condition by using twice dose of lentivirus compared with the single dose of this virus employed for [Figure 6B](#). Under this condition of high-dose infection, basal NSC Ex/Mv in the given amount was not enough to reduce viral infection; in contrast, induced NSC Ex/Mv in the same amount were effective to provide the antiviral action ([Figure 6C](#)). Thus, using an HIV-based lentivirus as another example of RNA viruses, murine NSC Ex/Mv have basal and induced antiviral actions, whereas the antiviral action of induced Ex/Mv is stronger.

### Antiviral Immunity of NSC Ex/Mv in Cell-Free Ambient Environment

Given that NSC Ex/Mv showed a cell-free innate antiviral effect against pseudotyped SARS-CoV-2 ([Figures 3](#) and [4](#)), we further examined if this finding could apply to HIV-based lentivirus. To do so, we incubated the purified lentiviruses with a type of purified NSC Ex/Mv in a buffer overnight and then fixed them for electron microscopic analysis. We obtained the morphological evidence suggesting that these NSC Ex/Mv

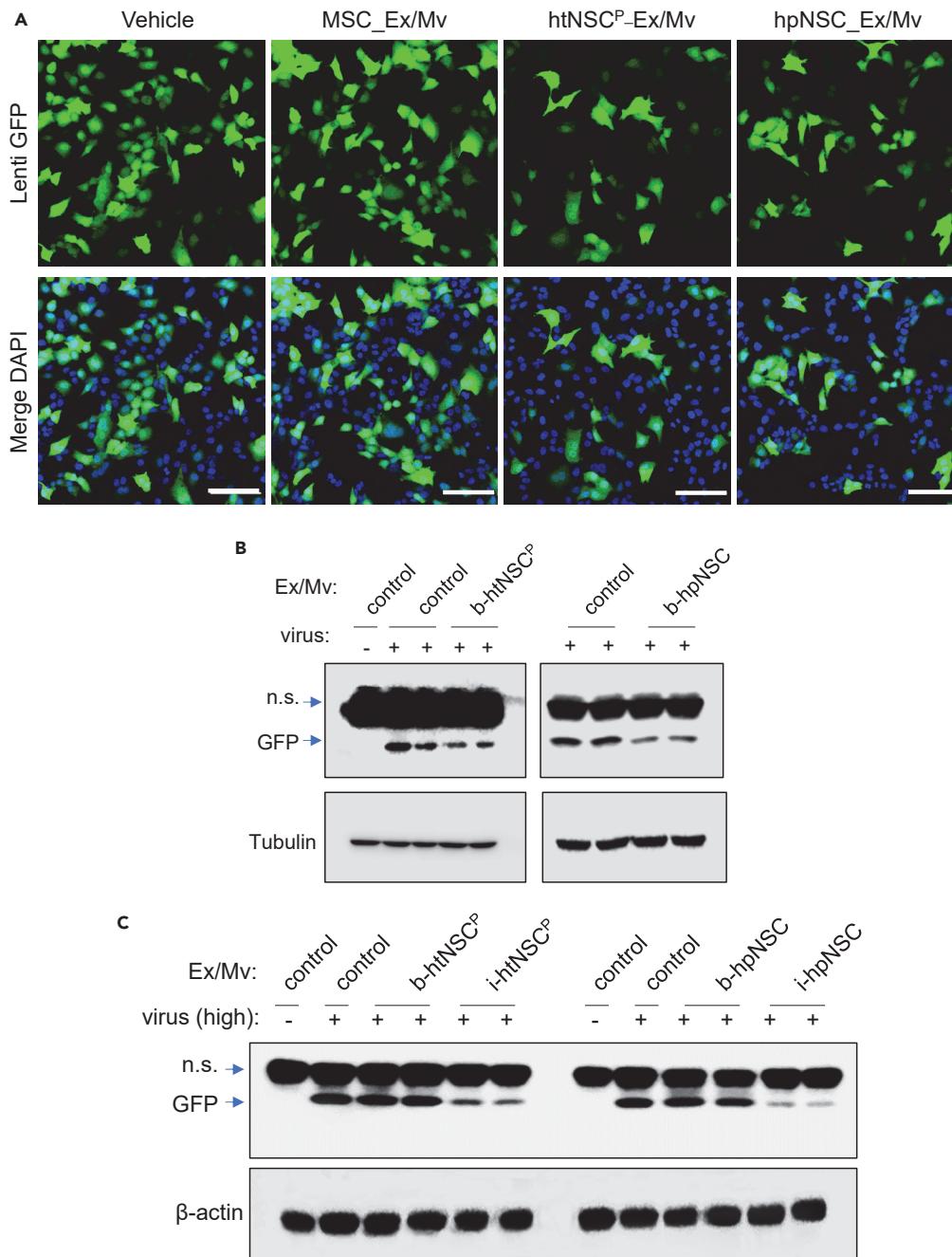


**Figure 6. Induced versus Basal NSC Ex/Mv against VSVG-Enveloped Lentivirus**

(A) Cultured A549 cells were infected with VSVG-incorporated GFP lentivirus in the presence or absence of Ex/Mv that were isolated from basal forms of NSC types and MSC as indicated, and 2 days later, these cells were fixed for GFP immunostaining. DAPI nuclear staining was included as a technical control. Scale bars, 100  $\mu$ m.

(B and C) Cultured A549 cells were infected with a standard (B) or high (C) dose of VSVG-enveloped GFP lentivirus in the presence or absence of Ex/Mv that were isolated from basal form (labelled by "b-") versus induced form (labelled by "i-") of NSC types as indicated, and 2 days later, these cells were harvested and lysed for western blot for GFP. Blot for  $\beta$ -tubulin or  $\beta$ -actin for the same membrane was included to provide a reference. n.s., non-specific.

physically interacted with lentiviruses leading to changes indicative of viral breakdown. These suggestive results are not presented, given that it was not always clear-cut to distinguish them because lentiviruses and exosomes were both round, although exosomes were often cup-shaped. Alternatively, we designed a biochemical assay to quantitatively assess this relationship in cell-free incubation condition. To do so, we incubated lentiviruses with NSC Ex/Mv versus vehicle in a buffer and then examined how this incubation could affect the viruses through western blotting for VSVG, which was the envelop protein of these lentiviruses. Also, to provide a time course profile, we designed several time points including 0.5, 4, and 24 h for Ex/Mv and lentivirus reaction in the buffer, compared with the virus or Ex/Mv alone in the same reaction condition. As shown in [Figures 7A and 7B](#), the mixture with basal NSC Ex/Mv from the hypothalamus and hippocampus both rapidly led to lentiviral degradation. This effect occurred as quickly as 0.5 h at room temperature, but interestingly longer time of incubation at 4°C did not further increase viral degradation. We similarly assessed the induced versions of NSC Ex/Mv and observed that they were comparable to basal NSC Ex/Mv in leading to degradation of VSVG lentiviruses. This similarity between basal and induced NSC Ex/Mv suggested that the cell-free antiviral actions of NSC Ex/Mv are innate immunity-like. Hence, these results in conjunction with findings in [Figures 1, 2, 3, and 4](#) further support the conclusion that murine NSC Ex/Mv have antiviral immunity actions intracellularly as well as extracellularly.

### NSC Ex/Mv piRNAs against HIV-Based Lentivirus and Their Adaptive Enrichment

Finally, we also analyzed piRNAs that might target the genome of the HIV-based lentivirus, which contained a few HIV genomic RNA segments including HIV long terminal repeats, psi, RRE, and  $\Delta$ U3 sequences, as elucidated in [Figure S6A](#). In addition, this lentiviral genome contained CMV promoter sequence and GFP-encoding sequence. Despite the fact that the RNA sequence of this recombinant lentivirus is rather short, we identified a list of piRNAs with at least 15 nucleotides matching with these viral sequences of which quite a few met Criteria 1 or 2 ([Table S3](#)). Through qPCR, we examined some of these piRNAs and found that they were present in NSC Ex/Mv but much less detectable in MSC Ex/Mv ([Figure S6B](#)). Furthermore, some of these NSC Ex/Mv piRNAs were also upregulated after a lentiviral pre-exposure to these NSC ([Figures S7A and S7B](#)). We also asked if GFP-encoding RNA sequence could have target piRNAs and if so whether they could be induced through a lentiviral pre-exposure. As shown in [Table S3](#), we found several mouse piRNAs that matched against either the sense or antisense sequence of GFP-encoding RNA. Using qPCR, we then measured a few of them and found that each was detectable in NSC Ex/Mv but much less detectable in MSC Ex/Mv (data not shown). Moreover, two of these GFP piRNAs were significantly upregulated in induced NSC Ex/Mv compared with basal NSC Ex/Mv ([Figure S7C](#)). All these results based on HIV lentivirus were consistent with piRNA adaptive enrichment as described above for pseudotyped SARS-CoV-2. Also, based on up-regulation of piRNAs against RNAs that encoded luciferase ([Figure S5](#)) and GFP ([Figure S7C](#)), the adaptive reaction of NSC Ex/Mv piRNA can target a newly incorporated sequence in a viral genome. Taken together, through sequence analysis and qPCR for multiple viral types and components, we obtained information suggesting that piRNAs could be involved in the antiviral actions of these NSC Ex/Mv.

## DISCUSSION

In this study, we showed that murine NSC Ex/Mv can provide innate and adaptive antiviral actions by testing pseudotyped SARS-CoV-2 and HIV-based recombinant lentivirus. As elucidated in [Figure 8](#), the antiviral effects of these Ex/Mv are predicted to comprise an intracellular action in host cells as well as an extracellular action through which Ex/Mv particles directly interact with viruses. Although these Ex/Mv contain other non-coding RNAs (such as miRNAs and long non-coding RNAs) and proteins/peptides that might have contributions, this study uncovered the possible importance of piRNAs for the antiviral immunity of these Ex/Mv.

In clinical studies, largely due to the limited availability of human NSC, the option of using human MSC has been considered for exosomal therapeutics, and recent studies of using MSC or their derived exosomes to target COVID-19 showed positive outcomes ([Bari et al., 2020](#); [Borger et al., 2020](#); [Gupta et al., 2020](#); [Jayaramayya et al., 2020](#); [Pinky et al., 2020](#); [Tsuchiya et al., 2020](#)), although it is unclear if these effects were related to a direct antiviral action or indirectly due to improved physiology which leads to resilience against viral infection. Given that NSCs are capable of abundantly producing Ex/Mv which were applicable ([Zhang et al., 2017](#)), our findings in this study further support the proposal that NSCs could be important for Ex/Mv therapeutics. Because of the various advantages of NSC exosomes including the pro-survival effects in fatal disease conditions ([Tang et al., 2020](#)), we predict that adding the application of NSC Ex/Mv will increase the coverage and effectiveness of exosome therapeutics. Furthermore, we observed that murine NSC Ex/Mv can provide a cell-free antiviral action against viruses, raising up the possibility that murine NSC Ex/Mv

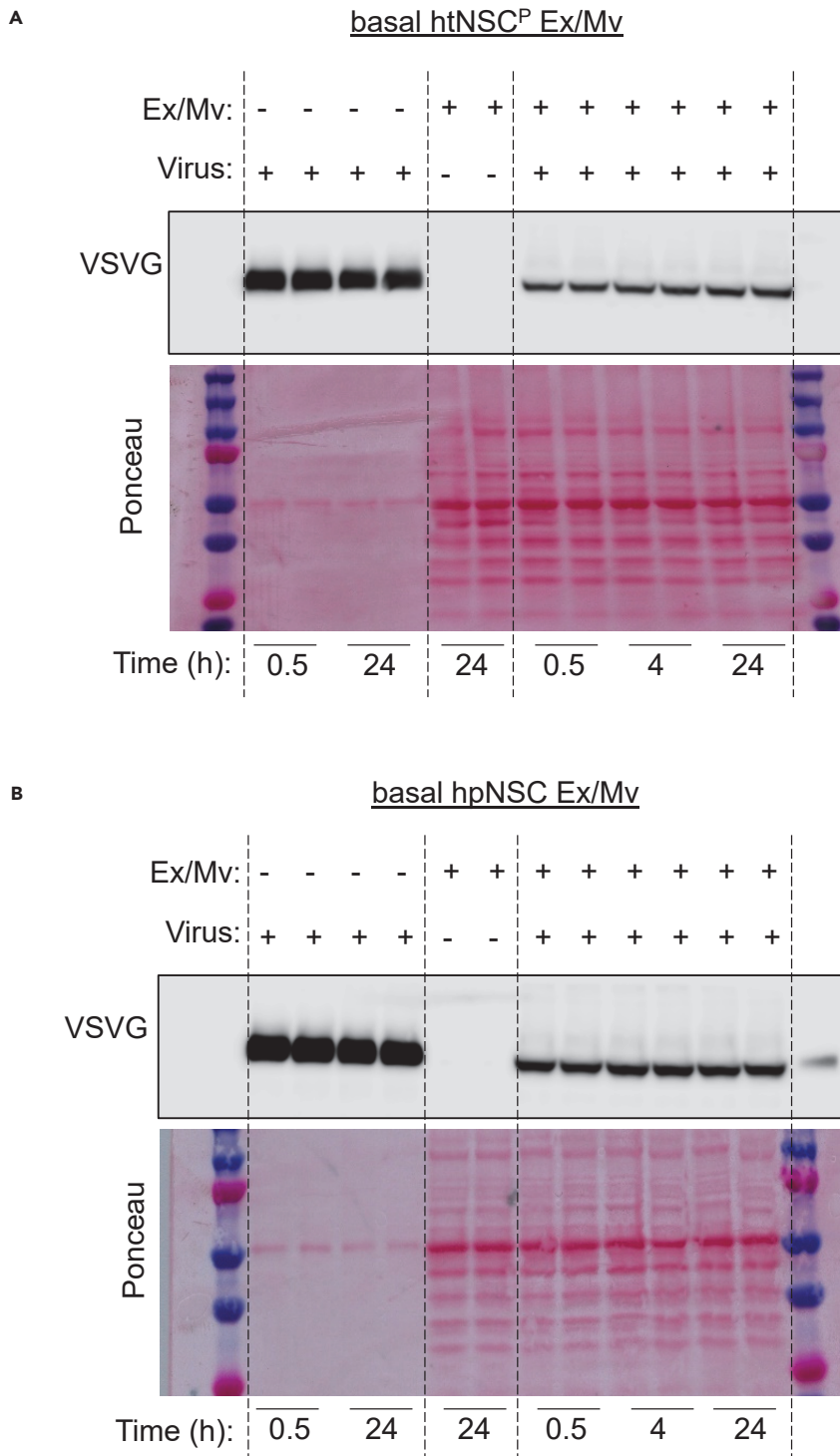


**Figure 7. Cell-Free Antiviral Effects of NSC Ex/Mv against HIV-Based Lentivirus**

(A and B) VSVG-enveloped GFP lentiviruses were mixed with basal Ex/Mv from htNSC<sup>P</sup> (labeled as htNSC<sup>P</sup>) (A) or hpNSC (B) for 0.5 h at room temperature and then 4–24 h at 4°C. These lentiviruses or Ex/Mv alone maintained under the same conditions were included as two control groups. These samples were then lysed and processed for western blot using an antibody against VSVG. Ponceau staining of duplicated gels under the same procedure was used as a technical control to reflect the protein distribution in these gels.

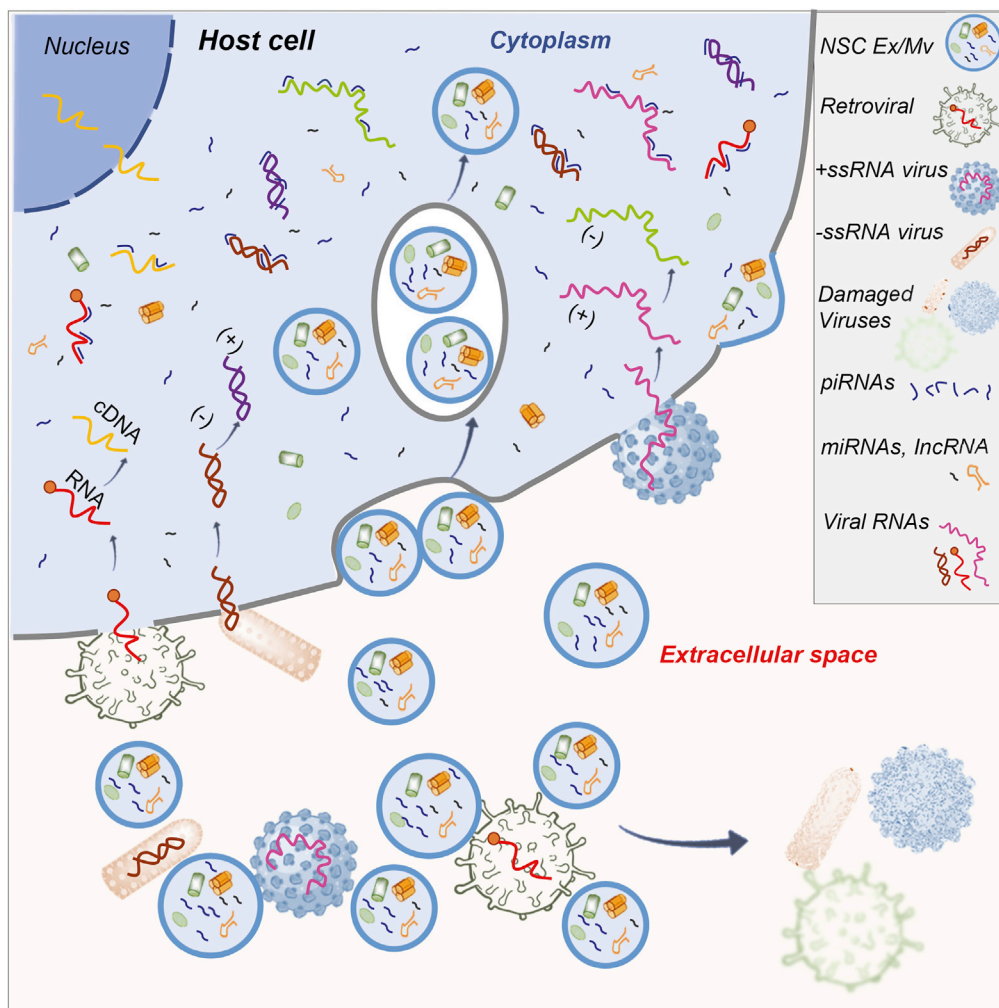


**Figure 8. Diagram for the Antiviral Immunity of NSC Ex/Mv**

The antiviral immunity of NSC-released Ex/Mv against various viruses (the same image is used as the Graphical Abstract of this article to provide the overall idea). These antiviral effects are suggested to comprise an intracellular action in infected host cells, which take Ex/Mv particles and their contents, as well as an extracellular action through which Ex/Mv particles directly interact with viruses despite the fact that the underlying intracellular and extracellular mechanisms are still unclear. Although NSC Ex/Mv contain other non-coding RNAs (such as miRNAs and long non-coding RNAs) and proteins/peptides, which might provide antiviral contributions, this study revealed that these Ex/Mv have a key feature of innately and even adaptively producing large families of piRNAs against genomes of various viruses, suggesting a possible important role of these special small RNAs for antiviral immunity. This study addressed a recombinant retrovirus and a negative-strand RNA virus, and although it did not investigate a positive-strand RNA virus such as wild-type SARS-CoV-2, this type of virus is proposed in this diagram based on piRNA sequence analysis.

could be used for humans through an external application such as nasal spray to break viruses such as SARS-CoV-2, despite little being known about the differences between the murine and human NSCs to date.

In this work, we further discovered that murine NSC Ex/Mv are characterized by producing a vast collection of diverse piRNA species including those that could potentially target genomes of several RNA viruses. These piRNA libraries might contain species for targeting against many other viruses including DNA viruses, which this study did not examine. Probably, this level of vast diversity is related to the heterogeneity of NSC population, which had been established in the history of life evolution. Indeed, we have previously appreciated that NSC is very heterogeneous (Tang et al., 2020); thus approaches such as single-cell analysis

will be valuable to reveal in-depth information and understandings. The notion of piRNA immunity and its enrichment through viral pre-exposure could lead to the extension of classical antibody-based adaptive immunity to small RNA-based disciplines. This feature can be clinically relevant, as vaccine development for RNA viruses is challenged by the situation that variants and mutations of RNA viruses are high, for instance, mutational and protein profile analyses revealed a large number of amino acid substitutions in SARS-CoV-2 indicating that the viral proteins are heterogeneous (Islam et al., 2020). Given this reality, the observed antiviral actions of NSC Ex/Mv and the possible role of piRNAs in antiviral immunity can provide the initial clues and ideas to promote future research for studying if NSC Ex/Mv and piRNAs could be developed to complement with antibody-based vaccine strategy and development.

Finally, this research provided a long list of representative piRNAs with the sequences matching against three different kinds of viral genomes, and we predict that at least some of them are likely important for the related antiviral actions of NSC Ex/Mv. The pool of piRNA sequences that match against viral genomes can be further expanded and examined based on the methodologies in this work. The sequence information of these piRNAs if verified for being antiviral will help guiding RNA-based vaccination strategies as well as exploring the underlying effects and mechanisms of these strategies. In this context, although we showed that NSC Ex/Mv are more important than MSC Ex/Mv for containing these piRNAs, we should point out that NSC might not be the only cell type for this feature, and to explore and find out other types of cells and even peripheral cells with this feature will be valuable for increasing the width and opportunity of potential applications against viral infection and diseases.

### Limitations of the Study

One limitation of this study is that our experiments evaluated only two recombinant laboratory viruses. Testing wild-type viruses such as coronavirus and HIV is important for future research. The second limitation is, this study was based on *in vitro* cell culture models, thus it is important to call for research of using animal models and human disease conditions to evaluate the predicted translational and pharmacological values of these findings. Also, whereas the antiviral actions of the induced versions of NSC Ex/Mv are stronger, basal versions of these extracellular vesicles seem effective only for some cell types, thus it is necessary to understand the underlying process, which is still unclear in this study. Third, the potential role of piRNAs was predicted based on sequence analysis and correlative experimental results (thus these results are presented in the [Supplemental Information](#)), so future studies are needed to verify if piRNAs per se can provide important antiviral actions. Finally, as this study focused on murine NSC Ex/Mv, which has its own significance such as the possible application, it should be more informative to compare them with human NSC Ex/Mv in terms of piRNAs and antiviral immunity.

### Resource Availability

#### Lead Contact

Dongsheng Cai, Department of Molecular Pharmacology, Albert Einstein College of Medicine; E-mail: [dongsheng.cai@einsteinmed.org](mailto:dongsheng.cai@einsteinmed.org).

#### Materials Availability

All materials, methodologies, protocols, and related information that were generated in this study are available upon request.

#### Data and Code Availability

This study did not involve code generation. All data and related experimental information from this study are available upon request.

## METHODS

All methods can be found in the accompanying [Transparent Methods supplemental file](#).

## SUPPLEMENTAL INFORMATION

Supplemental Information can be found online at <https://doi.org/10.1016/j.isci.2020.101806>.

## ACKNOWLEDGMENTS

The authors thank Cai laboratory personnel and the electron microscopy facilities of Icahn School of Medicine at Mount Sinai and Cold Spring Harbor Laboratory for technical assistance. This study was supported in part by Einstein internal resource/sponsorship and NIH AG031774 (all to D.C.).

## AUTHORS CONTRIBUTION

B.Y. performed experiments including cell models and culture, virus and Ex/Mv production and purification, western blot, immunostaining, and biochemical assays; did data analysis; and contributed to data interpretation. S.I. co-performed cellular, viral, and Ex/Mv experiments; did western blot; prepared plasmids; and contributed to data analysis and interpretation. C.R. performed small RNA isolation and qPCR and analyzed these data; X.Z. analyzed viral and piRNA sequences and designed piRNA primers. D.C. conceived all the ideas and concepts, designed the project (hypotheses, specific aims, experimental strategies, and methodologies), provided resources, organized and supervised the study, evaluated approaches, guided and led data analysis, led and finalized data interpretation, and wrote the paper.

## DECLARATION OF INTERESTS

The authors have no financial interests to declare. The results in this manuscript are under US provisional patent application.

Received: September 24, 2020

Revised: October 28, 2020

Accepted: November 10, 2020

Published: December 18, 2020

## REFERENCES

- Bari, E., Ferrarotti, I., Saracino, L., Perteghella, S., Torre, M.L., and Corsico, A.G. (2020). Mesenchymal stromal cell secretome for severe COVID-19 infections: premises for the therapeutic use. *Cells* 9, 924.
- Borger, V., Weiss, D.J., Anderson, J.D., Borrás, F.E., Bussolati, B., Carter, D.R.F., Dominici, M., Falcon-Perez, J.M., Gimona, M., Hill, A.F., et al. (2020). ISEV and ISCT statement on EVs from MSCs and other cells: considerations for potential therapeutic agents to suppress COVID-19. *Cytotherapy* 22, 482–485.
- Chen, M., Reed, R.R., and Lane, A.P. (2019). Chronic inflammation directs an olfactory stem cell functional switch from neuroregeneration to immune defense. *Cell Stem Cell* 25, 501–513 e505.
- Da Mesquita, S., Louveau, A., Vaccari, A., Smirnov, I., Cornelison, R.C., Kingsmore, K.M., Contarino, C., Onengut-Gumuscu, S., Farber, E., Raper, D., et al. (2018). Functional aspects of meningeal lymphatics in ageing and Alzheimer's disease. *Nature* 560, 185–191.
- Gupta, A., Kashite, S., Gupta, M., Rodriguez, H.C., Gautam, S.S., and Kadam, S. (2020). Mesenchymal stem cells and exosome therapy for COVID-19: current status and future perspective. *Hum. Cell* 33, 907–918.
- Hoffmann, M., Kleine-Weber, H., Schroeder, S., Krüger, N., Herrler, T., Erichsen, S., Schiergens, T.S., Herrler, G., Wu, N.-H., Nitsche, A., et al. (2020). SARS-CoV-2 cell entry depends on ACE2 and TMPRSS2 and is blocked by a clinically proven protease inhibitor. *Cell* 181, 271–280.e278.
- Islam, M.R., Hoque, M.N., Rahman, M.S., Alam, A., Akther, M., Puspo, J.A., Akter, S., Sultana, M., Crandall, K.A., and Hossain, M.A. (2020). Genome-wide analysis of SARS-CoV-2 virus strains circulating worldwide implicates heterogeneity. *Sci. Rep.* 10, 14004.
- Jayaramayya, K., Mahalaxmi, I., Subramaniam, M.D., Raj, N., Dayem, A.A., Lim, K.M., Kim, S.J., An, J.Y., Lee, Y., Choi, Y., et al. (2020). Immunomodulatory effect of mesenchymal stem cells and mesenchymal stem-cell-derived exosomes for COVID-19 treatment. *BMB Rep.* 53, 400–412.
- Kim, M.S., Yan, J., Wu, W., Zhang, G., Zhang, Y., and Cai, D. (2015). Rapid linkage of innate immunological signals to adaptive immunity by the brain-fat axis. *Nat. Immunol.* 16, 525–533.
- Louveau, A., Smirnov, I., Keyes, T.J., Eccles, J.D., Rouhani, S.J., Peske, J.D., Derecki, N.C., Castle, D., Mandell, J.W., Lee, K.S., et al. (2015). Structural and functional features of central nervous system lymphatic vessels. *Nature* 523, 337–341.
- Ma, D., Chen, C.-B., Jhanji, V., Xu, C., Yuan, X.-L., Liang, J.-J., Huang, Y., Cen, L.-P., and Ng, T.K. (2020). Expression of SARS-CoV-2 receptor ACE2 and TMPRSS2 in human primary conjunctival and pterygium cell lines and in mouse cornea. *Eye* 34, 1212–1219.
- Moseman, E.A., Blanchard, A.C., Nayak, D., and McGavern, D.B. (2020). T cell engagement of cross-presenting microglia protects the brain from a nasal virus infection. *Sci. Immunol.* 5, eabb1817.
- Nie, J., Li, Q., Wu, J., Zhao, C., Hao, H., Liu, H., Zhang, L., Nie, L., Qin, H., Wang, M., et al. (2020). Establishment and validation of a pseudovirus neutralization assay for SARS-CoV-2. *Emerg. Microbes Infect.* 9, 680–686.
- Papadopoulos, Z., Herz, J., and Kipnis, J. (2020). Meningeal lymphatics: from anatomy to central nervous system immune surveillance. *J. Immunol.* 204, 286–293.
- Pavlov, V.A., Chavan, S.S., and Tracey, K.J. (2018). Molecular and functional neuroscience in immunity. *Annu. Rev. Immunol.* 36, 783–812.
- Pinky, Gupta, S., Krishnakumar, V., Sharma, Y., Dinda, A.K., and Mohanty, S. (2020). Mesenchymal stem cell derived exosomes: a nano platform for therapeutics and drug delivery in combating COVID-19. *Stem Cell Rev. Rep.* 13, 1–11.
- Rosas-Ballina, M., Olofsson, P.S., Ochani, M., Valdes-Ferrer, S.I., Levine, Y.A., Reardon, C., Tusche, M.W., Pavlov, V.A., Andersson, U., Chavan, S., et al. (2011). Acetylcholine-synthesizing T cells relay neural signals in a vagus nerve circuit. *Science* 334, 98–101.
- Shen, E.Z., Chen, H., Ozturk, A.R., Tu, S., Shirayama, M., Tang, W., Ding, Y.H., Dai, S.Y., Weng, Z., and Mello, C.C. (2018). Identification of piRNA binding sites reveals the argonaute regulatory landscape of the *C. elegans* germline. *Cell* 172, 937–951.e918.
- Tang, Y., Zuniga-Hertz, J.P., Han, C., Yu, B., and Cai, D. (2020). Multifaceted secretion of htNSC-derived hypothalamic islets induces survival and



antidiabetic effect via peripheral implantation in mice. *Elife* 9, e52580.

Tsuchiya, A., Takeuchi, S., Iwasawa, T., Kumagai, M., Sato, T., Motegi, S., Ishii, Y., Koseki, Y., Tomiyoshi, K., Natsui, K., et al. (2020). Therapeutic potential of mesenchymal stem cells and their exosomes in severe novel coronavirus disease 2019 (COVID-19) cases. *Inflamm. Regen.* 40, 14.

Wang, J., Zhang, P., Lu, Y., Li, Y., Zheng, Y., Kan, Y., Chen, R., and He, S. (2019). piRBase: a

comprehensive database of piRNA sequences. *Nucleic Acids Res.* 47, D175–D180.

Wang, K., Yaghi, O.K., Spallanzani, R.G., Chen, X., Zemmour, D., Lai, N., Chiu, I.M., Benoist, C., and Mathis, D. (2020). Neuronal, stromal, and T-regulatory cell crosstalk in murine skeletal muscle. *Proc. Natl. Acad. Sci. U S A* 117, 5402–5408.

Whitt, M.A. (2010). Generation of VSV pseudotypes using recombinant DeltaG-VSV for studies on virus entry, identification of

entry inhibitors, and immune responses to vaccines. *J. Virol. Methods* 169, 365–374.

Zhang, D., Tu, S., Stubna, M., Wu, W.S., Huang, W.C., Weng, Z., and Lee, H.C. (2018). The piRNA targeting rules and the resistance to piRNA silencing in endogenous genes. *Science* 359, 587–592.

Zhang, Y., Kim, M.S., Jia, B., Yan, J., Zuniga-Hertz, J.P., Han, C., and Cai, D. (2017). Hypothalamic stem cells control ageing speed partly through exosomal miRNAs. *Nature* 548, 52–57.

iScience, Volume 23

## **Supplemental Information**

**Innate and Adaptive Immunity of Murine Neural  
Stem Cell-Derived piRNA Exosomes/Microvesicles  
against Pseudotyped SARS-CoV-2 and HIV-Based Lentivirus**  
Bin Yu, Shoeb Ikhlas, Chunsheng Ruan, Xingxing Zhong, and Dongsheng Cai

## Transparent Methods

### Cell culture

**Primary NSC models and culture:** Primary culture of NSCs was performed as described previously (Li et al., 2012; Yu et al., 2020; Zhang et al., 2017). In brief, the hypothalamus or hippocampus was dissected from newborn C57BL/6 mice, cut into small pieces of approximately 1 mm<sup>3</sup>, and followed by digestion using TrypLE Express enzyme (Life Technologies) for 10 min at 37 °C. After centrifugation, cells were suspended in NSC medium composed of neurobasal-A (Life Technologies), 0.25% GlutaMAX supplement (Life Technologies), 2% B27 without vitamin A (Life Technologies), 10 ng ml<sup>-1</sup> EGF (Sigma-Aldrich), 10 ng ml<sup>-1</sup> bFGF (Life Technologies) and 1% penicillin–streptomycin and seeded in ultralow-adhesion 6-well plates (Corning). One week later, neurospheres were collected by centrifugation and trypsinized with TrypLE Express enzyme into single cells, passaged and maintained in neurosphere culture. All procedures of involving animal uses were approved by the Institutional Care and Use Committee of Albert Einstein College of Medicine (protocol #20171210, #20170812, #20171209, #20171208, #00001111). **NSC lines:** The line of htNSC<sup>PGHM</sup> was established in our previous research (Tang et al., 2020). NSC cell lines of stably overexpressing hACE2 were generated by hACE2 lentivirus transduction for two days and puromycin-based selections for one week. Lentivirus or pseudotyped SARS-CoV-2 stimulated NSC lines for adaptive immunity-like response study were generated by persistent viral infection with 2 µl virus per 10<sup>6</sup> cells for 2 generations, followed by normal NSC media culture. **Other cell lines:** Mouse mesenchymal stem cell (MUBMX-01001, Cyagen) was cultured in MSC medium (MUXMX-90011, Cyagen). HEK293T (CRL-3216, ATCC), HepG2 (HB-8065, ATCC) and BHK21 (EH1011, Kerfast) cells were incubated in Dulbecco's modified Eagle

medium (ThermoFisher Scientific). A549 (CCL-185, ATCC) was cultured in DMEM/F-12 Medium (ATCC). Calu3 (HTB-55, ATCC) was cultured in Minimum Essential Medium (ATCC). Except NSC culture medium which was serum-free, all other culture media were supplemented with 5-10% heat-inactivated fetal bovine serum (Sigma) or MSC specific fetal bovine serum (Cyagen), 100 U/mL of penicillin and streptomycin (Gibco). Ex/Mv-free serum (through ultracentrifugation) was used for experiments involving Ex/Mv collection and analysis. For seeding and sub-culture, cells were first washed with phosphate buffered saline (PBS) and then incubated in the presence of trypsin/EDTA solution (Life Technologies) until cells detached. BHK21 was cultured at 37°C and 7% CO<sub>2</sub> in a humidified atmosphere, while all other cell lines were cultured at 37°C and 5% CO<sub>2</sub> in a humidified atmosphere.

### **Ex/Mv isolation and purification**

Ex/Mv in MSC and NSC cell culture media were purified by differential centrifugation as described previously (Zaborowski et al., 2015). In brief, culture medium was processed by ultracentrifugation at 100,000 g, 4°C overnight to remove particles to generate exosome-free medium. Cells were cultured in exosome-free medium for two days, after which the medium was collected, centrifuged to remove cells and large debris. The supernatant was collected and centrifuged at 2000 g for 10 min to remove small debris, immediately followed by Ex/Mv isolation in 4°C, then filtered through 0.8 µm pore-size filter for Ex/Mv or 0.2 µm pore-size filter for exosomes only. The filtrate was collected and ultra-centrifuged at 100,000g for 70 min to pellet down particles and re-suspended with PBS.

### **Plasmids and virus production**

All procedures related to virus production were handled under biosafety level 2 and approved by institutional biosafety committee. The lentiviral vector of CMV-promoter-driven GFP was studied previously (Li et al., 2012). The lentiviral vector of EF1A-promoter-driven hACE2 (VB200000-2751mcf) was purchased from Vector Builder. Vector pCAGGS containing the SARS-Related Coronavirus 2, Wuhan-Hu-1 spike glycoprotein gene (NR-52310) was obtained from BEI Resources. pCAGGS-G-Kan plasmid (EH1017) was purchased from Kerafast. Lentiviruses were produced by transfecting HEK293T cells with corresponding viral and packaging plasmids, purified by ultracentrifugation as described previously (Tang et al., 2020; Yu et al., 2020; Zhang et al., 2017). Pseudotyped  $\Delta$ G-luciferase rVSV (EH1025-PM) was purchased from Kerafast. Generation of pseudotyped  $\Delta$ G-luciferase rVSV or pseudotypes with SARS-CoV-2 glycoprotein was performed as previous described (Whitt, 2010). In briefly, BHK-21 cells were transfected with pCAGGS-G-Kan or SARS-CoV-2 spike glycoprotein plasmid and 24 hrs later infected with  $\Delta$ G-luciferase rVSV. Culture supernatants were harvested at 24 hrs post-infection for ultracentrifuge with 20% sucrose cushion at 100,000g for 35 min. The recombinant lentiviruses, rVSV or pseudotyped SARS-CoV-2 viruses were reconstituted in a small volume of PBS to achieve a 1000X concentration.

## **Western blot**

**Cell samples preparation:** Cell lysate was prepared by sonication in ice-cold RIPA lysis buffer (20 mM Tris-HCl, pH 7.4, 10 mM NaCl, 1 mM EDTA, 0.01 % SDS, 1 % Triton X-100 and 1x protease inhibitor cocktail). After protein concentration determined, cell lysate samples were boiling in sample buffer at 95 °C for 5 min. **Ex/Mv and virus pre-mixture study:** 25  $\mu$ g Ex/Mv that were isolated from NSC-secreted media were mixed with 1 $\mu$ l

lentivirus or 5µl pseudovirus SARS2-luciferaseVSV. The mixtures incubated for designed time and at designed temperature were mixed with sample buffer and boiled at 95 °C for 5 min, then used for western blot to analysis VSV-G or SAR-CoV-2 glycoprotein level.

**Western blotting:** The boiled protein samples were separated by SDS-PAGE and were transferred onto 0.2 µm PVDF membrane. After blocked by 5% non-fat milk in TBST, the membranes were blotted with anti-PIWIL2 rabbit pAb (ab36764, Abcam), anti-CD81 mouse mAb (sc-23962, Santa Cruz), anti-TSG101 mouse mAb (sc-7964, Santa Cruz), anti-GFP rabbit pAb (NB600-308, Novus Biologicals), anti-β-Actin rabbit pAb (4967S, Cell signaling Technology), anti-Tubulin mouse mAb (4466, Cell signaling Technology) anti-VSVG rabbit pAb (NB1002485, Novus Biologicals) or anti-SAR2-CoV-2 S human mAb (NR-52392, BEI) for overnight at 4°C, followed by HRP-conjugated goat anti-rabbit (7074, Cell Signaling Technology), anti-mouse (7076, Cell Signaling Technology) or anti-human (PI31410, Invitrogen) secondary antibody. Ponceau S staining (Sigma, #P7170) was used as total protein loading control. Image J software was used for quantitatively analysis.

### **piRNA analysis**

Different sense and antisense segments of viral RNA sequence were based on lentiviral CMV-promoter-driven-GFP vector (Thermo Fisher), pseudotyped ΔG-luciferase rVSV genome (Karafast, Thermo Fisher), and SARS2-CoV-2, Wuhan-Hu-1 genome (NC\_045512.2). Mouse piRNA database (piRNAQuest) was used for piRNA screening according to the literature (Sarkar et al., 2014). Continuous alignment of 14-16 nucleotides and above with target RNA was set up to generate an initial list of piRNAs, which were then further aligned against a target RNA sequence to manually examine the total number of nucleotide matches as well as position-wide nucleotide matches. Criteria # 1 required perfect match for the primary seed

sequence (piRNA nucleotides 2–11) and allowed no more than 4 mismatches in the secondary seed sequence (piRNA nucleotides 12–21), and Criteria #2 allowed 5 mismatches in the secondary lead sequence but still required perfect matches for primary seed sequence.

### **Ex/Mv small RNA isolation and qPCR**

Ambion mirVana miRNA isolation kit (AM1560) was used to isolate small RNA from purified Ex/Mv, following manufacturer's guidelines. RNA concentration and purity were measured at 260 nm and 280 nm absorbance using the Nanodrop spectrophotometer. Extracted small RNA were polyadenylated and reverse transcribed to cDNA (Shi et al., 2012) using the Lucigen poly(A) polymerase tailing kit (PAP5104H) and RevertAid RT reverse transcription kit (K1691), then subjected to real-time qPCR with specific primers, universal primer and SYBR Green PCR Master Mix. Specific primers were designed using sRNAPrimerDB module (Xie et al., 2019). All qPCR results of comparing NSC with MSC were based on the same amount of Ex/Mv total small RNA and did not involve U6 normalization because NSC and MSC have dramatical difference in U6 expression which is thus not suitable for being used as an internal control for different cell types. All qPCR results of comparing basal and induced Ex/Mv of the same NSC type were normalized according to U6 levels to reflect the relative changes between a specific piRNA target and non-specific small RNA. Primer sequences were listed in Table S4.

### **Immunostaining**

**Cell preparation:** NSCs were seed on laminin-coated coverslips. After reaching 70% confluence, cells were fixed 15 min at room temperature with 4% PFA. A549 cells were seeded on polylysine-coated coverslips in 24-well plates and treated by 0.02-0.1  $\mu$ l lentivirus and 3-5  $\mu$ g exosomes or PBS, 72 hrs after seeding, cells were fixed with 4% PFA for 15 min at room

temperature before immunostaining. A549, HepG2 or Calu3 were seeded on polylysine-coated coverslips in 24-well plates, and treated by 1  $\mu$ l pseudotyped SARS-CoV-2 virus and 3  $\mu$ g exosomes or PBS, 24 hrs after seeding, cells were fixed with 4% PFA for 15 min at room temperature before immunostaining. **Exosome preparation:** Purified exosomes isolated from NSCs or MSC were seed on polylysine-coated coverslips and fixed. **Immunofluorescence staining:** Cells and exosomes immunofluorescence staining were conducted as previous described (Kadiu et al., 2012; Tang et al., 2020). In briefly, specimen was washed three times in cold PBS and incubated 30 min in permeabilization buffer (Triton X-100 0.1%, Goat serum 5%, PBS). Cells were incubated overnight at 4°C with primary antibodies against PIWIL2 (ab36764, Abcam), CD81 (sc-23962, Santa Cruz), TSG101 (sc-7964, Santa Cruz), GFP (NB600-308, Novus Biologicals), Luciferase (NB600307, Novus Biologicals), and human ACE2 (MA5-32307). Cells or exosomes were incubated in secondary antibodies (Goat anti-rabbit, goat anti-mouse conjugated with Alexa Fluor 488 and 555, respectively, Invitrogen) and after 3 times of wash with cold PBS were mounted (VECTA-SHIELD mounting media with DAPI). Images were captured using Leica SP8 confocal microscope and analyzed by FIJI software.

### **Luciferase assay**

A549, HepG2 or Calu3 cells seeded in 24-well plates ( $5 \times 10^4$  cells per well) were incubated with 1  $\mu$ l pseudotyped SARS-CoV-2 virus (wildtype SARS-CoV-2 spike protein incorporated  $\Delta$ G-luciferase-VSV) and 3  $\mu$ g exosomes, or the mixture of pseudotyped SARS-CoV-2 virus and exosomes which pre-incubation at 4°C overnight. 24 hrs after infection, cells were harvested and washed 3 times by PBS. The expression of firefly luciferase was quantitatively measured by



Roche Luciferase reporter gene assay (11669893001). Light emission within 10s after adding luciferase assay reagent was measured by Monolight 3010 luminometer.

### **Electronic microscopy**

Exosomes were filtered and purified by ultracentrifuge with 30% sucrose cushion at 100,000g for 90 min, followed by washing the exosome containing sucrose layer to pellet down the exosomes by diluting with phosphate-buffered saline and ultracentrifugation at 100,000g for 90 min (Gupta et al., 2018). 30  $\mu$ l exosomes extracted from NSCs supernatant, pseudotyped SARS-CoV-2 or lentivirus, or the mixture of exosomes with the viruses were incubated overnight (~0.5 hour at room temperature followed by 4°C) and then were used for structural analysis by transmission electron microscope (TEM). Grids preparation, uranyl acetate negative staining and transmission electron microscopy were performed at the Microscopy Core and Advanced Bioimaging Center, Icahn School of medicine at Mount Sinai and the St. Giles Foundation Advanced Microscopy Center, Cold Spring Harbor Laboratory.

### **Statistics and reproducibility**

All measured data were presented as mean  $\pm$  SEM. All quantitative experiments in this study were repeated independently and complementarily while the presentation was based on the data from representative single experiment per research question. Blindness and randomness were employed for obtaining and observing TEM images. Two-tailed unpaired Student's t-test was used for data analyses which involved only two groups for comparison, and ANOVA and Tukey's post-hoc tests were used for data analyses which involved more than two groups for

comparisons. Software for performing statistics included Prism and Matlab, and p value of less than 0.05 was considered statistically significant.

## References:

- Gupta, S., Rawat, S., Arora, V., Kottarath, S.K., Dinda, A.K., Vaishnav, P.K., Nayak, B., and Mohanty, S. (2018). An improvised one-step sucrose cushion ultracentrifugation method for exosome isolation from culture supernatants of mesenchymal stem cells. *Stem Cell Res Ther* 9, 180-180.
- Kadiu, I., Narayanasamy, P., Dash, P.K., Zhang, W., and Gendelman, H.E. (2012). Biochemical and Biologic Characterization of Exosomes and Microvesicles as Facilitators of HIV-1 Infection in Macrophages. *The Journal of Immunology* 189, 744.
- Li, J., Tang, Y., and Cai, D. (2012). IKK $\beta$ /NF- $\kappa$ B disrupts adult hypothalamic neural stem cells to mediate a neurodegenerative mechanism of dietary obesity and pre-diabetes. *Nat Cell Biol* 14, 999.
- Sarkar, A., Maji, R.K., Saha, S., and Ghosh, Z. (2014). piRNAQuest: searching the piRNAome for silencers. *BMC Genomics* 15, 555.
- Shi, R., Sun Yh Fau - Zhang, X.-H., Zhang Xh Fau - Chiang, V.L., and Chiang, V.L. (2012). Poly(T) adaptor RT-PCR. *Methods Mol Biol* 822, 53-66.
- Tang, Y., Zuniga-Hertz, J.P., Han, C., Yu, B., and Cai, D. (2020). Multifaceted secretion of htNSC-derived hypothalamic islets induces survival and antidiabetic effect via peripheral implantation in mice. *Elife* 9.
- Whitt, M.A. (2010). Generation of VSV pseudotypes using recombinant  $\Delta$ G-VSV for studies on virus entry, identification of entry inhibitors, and immune responses to vaccines. *J Virol Methods* 169, 365-374.
- Xie, S., Zhu, Q., Qu, W., Xu, Z., Liu, X., Li, X., Li, S., Ma, W., Miao, Y., Zhang, L., *et al.* (2019). sRNAPrimerDB: comprehensive primer design and search web service for small non-coding RNAs. *Bioinformatics* 35(9), 1566-1572.
- Yu, B., Tang, Y., and Cai, D. (2020). Brain is an endocrine organ through secretion and nuclear transfer of parathyrosin. *Life Science Alliance* 3, e202000917.
- Zaborowski, M.P., Balaj, L., Breakefield, X.O., and Lai, C.P. (2015). Extracellular Vesicles: Composition, Biological Relevance, and Methods of Study. *BioScience* 65, 783-797.
- Zhang, Y., Kim, M.S., Jia, B., Yan, J., Zuniga-Hertz, J.P., Han, C., and Cai, D. (2017). Hypothalamic stem cells control ageing speed partly through exosomal miRNAs. *Nature* 548, 52-57.

## Supplemental Figures

### Figure S1. Murine NSC Ex/Mv piRNAs potentially against SARS-CoV-2 genome (Related to Figure 1-5)

**A**, Schematic diagram depicting mouse piRNAs which potentially target the sense or antisense sequence of SARS-CoV-2 genome. Small bars indicate piRNAs that have the matched sequences with the adjacent viral RNA strand and thus complementary match with the other RNA strand, red font indicates piRNAs fitting with Criteria 1, green font indicates piRNAs with Criteria 2, and black font indicates piRNAs that with at least 16 nt matches but did not meet Criteria 1 or 2. The drawn lengths of viral genomic segments are not proportional to their actual sizes. For Orflab and spike sequences, the presentation includes only piRNAs which met Criteria 1 or 2. **B**, Ex/Mv were isolated and purified from htNSC<sup>PGHM</sup> (labelled as htNSC<sup>P</sup>), hpNSC and MSC, and the same amount of total small RNA from these Ex/Mv were examined by qPCR for a list of piRNAs which could potentially target SARS-CoV-2 genome. Data of each piRNA were expressed as the fold changes relative to the average values of MSC (the average values of MSC were all adjusted as 1). Information on sequences and labels of these piRNAs are detailed in Table S1. \* $p < 0.05$ , \*\* $p < 0.01$ , \*\*\* $p < 0.001$ , \*\*\*\* $p < 0.0001$ ; ANOVA/post-hoc, compared between indicated groups,  $n = 3$  independent biological samples per group, values represent the mean  $\pm$  s.e.m.

### Figure S2. Murine NSC Ex/Mv piRNAs potentially against pseudotyped SARS-CoV-2 genome (Related to Figure 1-5)

**A**, Schematic diagram depicting mouse piRNAs which potentially target the sense or antisense sequence of pseudotyped SARS-CoV-2 genome (SARS-CoV-2 spike protein enveloped  $\Delta$ G-luc-

VSV). Small bars indicate piRNAs that have the matched sequences with the adjacent viral RNA strand and thus complementary match with the other RNA strand), red font indicates piRNAs fitting with Criteria 1, green font indicates piRNAs with Criteria 2, and black font indicates piRNAs that with at least 16 nt matches but did not meet Criteria 1 or 2. The drawn lengths of viral genomic segments are not proportional to their actual sizes. **B**, Ex/Mv were isolated and purified from htNSC<sup>PGHM</sup> (labelled as htNSC<sup>P</sup>), hpNSC and MSC, and the same amount of total small RNA from these Ex/Mv were examined by qPCR for a list of piRNAs which could potentially target pseudotyped SARS-CoV-2 genome. Data of each piRNA were expressed as the fold changes relative to the average values of MSC (the average values of MSC were all adjusted as 1). Please see Fig. S4 for additional piRNAs in this experiment. Information on sequences and labels of these piRNAs are detailed in Table S2. \* $p < 0.05$ , \*\* $p < 0.01$ , \*\*\* $p < 0.001$ , \*\*\*\* $p < 0.0001$ ; ANOVA/post-hoc, compared between indicated groups,  $n = 3$  independent biological samples per group, values represent the mean  $\pm$  s.e.m.

**Figure S3. Additional NSC Ex/Mv piRNAs potentially against pseudotyped SARS-CoV-2 (Related to Figure 1-5)**

This supplemental Figure presents additional piRNAs potentially against pseudotyped SARS-CoV-2 genome compared among Ex/Mv isolated and purified from htNSC<sup>PGHM</sup> (labelled as htNSC<sup>P</sup>), hpNSC and MSC, as described in Fig. S2B. Please refer to Table S2 for detailed information of these piRNAs. \* $p < 0.05$ , \*\* $p < 0.01$ , \*\*\* $p < 0.001$ , \*\*\*\* $p < 0.0001$ ; ANOVA/post-hoc, compared between indicated groups,  $n = 3$  independent biological samples per group, values represent the mean  $\pm$  s.e.m.

**Figure S4. Induced NSC Ex/Mv piRNAs by pseudotyped SARS-CoV-2 stimulation (Related to Figure 1-5)**

Cultured hACE2-expressing htNSC were incubated with a pseudotyped SARS-CoV-2 (wildtype SARS-CoV-2 spike protein enveloped  $\Delta$ G-luc-VSV) for 2 generations and then returned to normal culture without virus for 5 generations before experiments (labelled as “induced”). These cells under the same procedure except viral infection were used as the baseline control (labelled as “basal”). Ex/Mv were isolated and purified from these basal and induced NSCs, and the same amount of total small RNA from these Ex/Mv were examined by qPCR for a list of piRNAs which could potentially target this pseudotyped SARS-CoV-2 genome. Expression level of each piRNA in both groups was normalized by expression level of U6 to reflect the relative change of target piRNA against non-target small RNA (represented by U6 expression), and then the values in induced group were expressed as fold changes relative to the average values in basal group (the average values of the basal group were all adjusted as 1). Please refer to Table S2 for detailed information of these piRNAs.  $*p < 0.05$ ,  $**p < 0.01$ ,  $***p < 0.001$ ,  $****p < 0.0001$ ; two-tailed Student’s t-test, compared between induced and basal groups,  $n = 4$  independent biological samples per group, values represent the mean  $\pm$  s.e.m.

**Figure S5. Murine NSC Ex/Mv piRNAs potentially against luciferase RNA sequence (Related to Figure 1-5)**

This suppl. Figure presents information on piRNAs that potentially target the sense or antisense of luciferase RNA sequence. **A**, Comparisons among Ex/Mv of htNSC<sup>PGHM</sup> (labelled as htNSC<sup>P</sup>), hpNSC and MSC, as described in Fig. S2B. **B**, Comparison between Ex/Mv from basal vs. induced htNSC<sup>PGHM</sup>, as described in Fig. S4.  $*p < 0.05$ ,  $**p < 0.01$ ,  $***p < 0.001$ ;

ANOVA/post-hoc (A) and two-tailed Student's t-test (B), compared between indicated groups, n = 3–4 independent biological samples per group, values represent the mean ± s.e.m.

**Figure S6. Murine NSC Ex/Mv piRNAs potentially against HIV-based lentiviral genome (Related to Figure 5-7)**

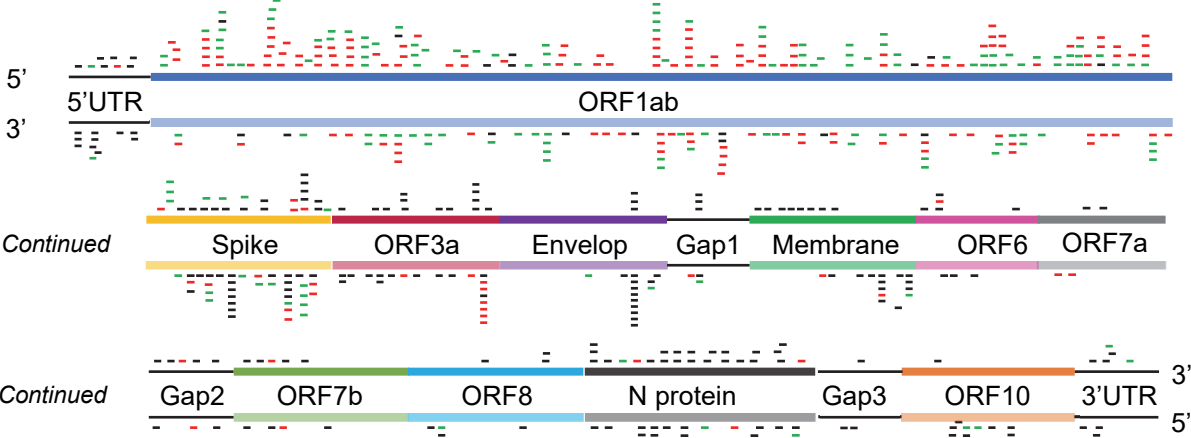
**A**, Schematic diagram depicting mouse piRNAs which potentially target against the sense or antisense sequence of recombinant lentiviral genome. Small bars indicate piRNAs that have the matched sequences with the adjacent viral RNA strand and thus complementary match with the other RNA strand), red font indicates piRNAs fitting with Criteria 1, and green font indicates piRNAs with Criteria 2, and black font indicates piRNAs that with at least 16 nt matches but did not meet Criteria 1 or 2. The drawn lengths of viral genomic segments are not proportional to their actual sizes. 5'-LTR and 3'-LTR are based on the same genomic sequences and piRNAs. **B**, Ex/Mv were isolated and purified from htNSC<sup>PGHM</sup> (labelled as htNSC<sup>P</sup>), hpNSC and MSC, and the same amount of total small RNA from these Ex/Mv were examined by qPCR for a list of piRNAs which could potentially target a lentiviral genome. Data of each piRNA were expressed as the fold changes relative to the average values of MSC (the average values of MSC were all adjusted as 1). Information on sequences and labels of these piRNAs are detailed in Table S3. \* $p < 0.05$ , \*\* $p < 0.01$ , \*\*\* $p < 0.001$ , \*\*\*\* $p < 0.0001$ ; ANOVA/post-hoc, compared between indicated groups, n = 3 independent biological samples per group.

**Figure S7. Induced vs. basal NSC Ex/Mv piRNAs against HIV-based lentiviral genome (Related to Figure 5-7)**

Cultured htNSC<sup>PGHM</sup> (labelled as htNSC<sup>P</sup>) or hpNSC were incubated with a VSVG-enveloped GFP lentivirus for 2 generations and then returned to normal culture for 5 generations before experiments. These cells under the same procedure except viral infection were used as the basal control. Ex/Mv were isolated and purified from these basal and induced NSCs, and the same amount of total small RNA from these Ex/Mv were examined by qPCR for a list of piRNAs which could potentially target this lentiviral RNA genome (**A, B**) or GFP RNA (**C**). Data of each piRNA in both groups were normalized with U6 expression levels to reflect the relative changes of target piRNA against non-target small RNA (represented by U6 expression) and then the values in induced group were expressed as fold changes relative to the average values of basal group (the average values of the basal group were all adjusted as 1). Please refer to Table S3 for detailed information of these piRNAs. \* $p < 0.05$ , \*\* $p < 0.01$ , \*\*\* $p < 0.001$ , \*\*\*\* $p < 0.0001$ ; two-tailed Student's t-test, compared between induced and basal groups,  $n = 4$  independent biological samples per group, values represent the mean  $\pm$  s.e.m.

Figure S1

A Murine piRNAs against SARS-CoV-2



B

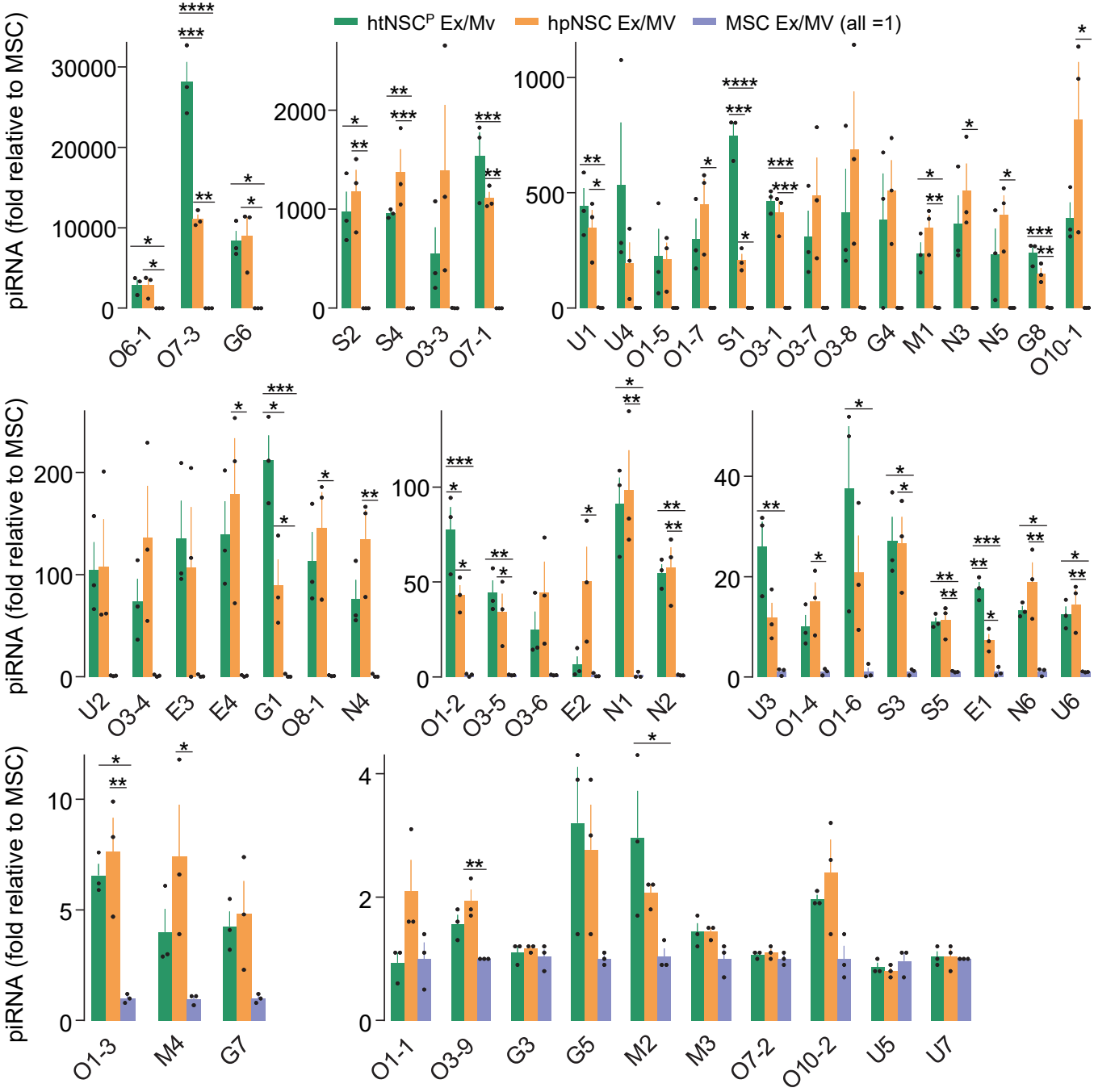




Figure S2

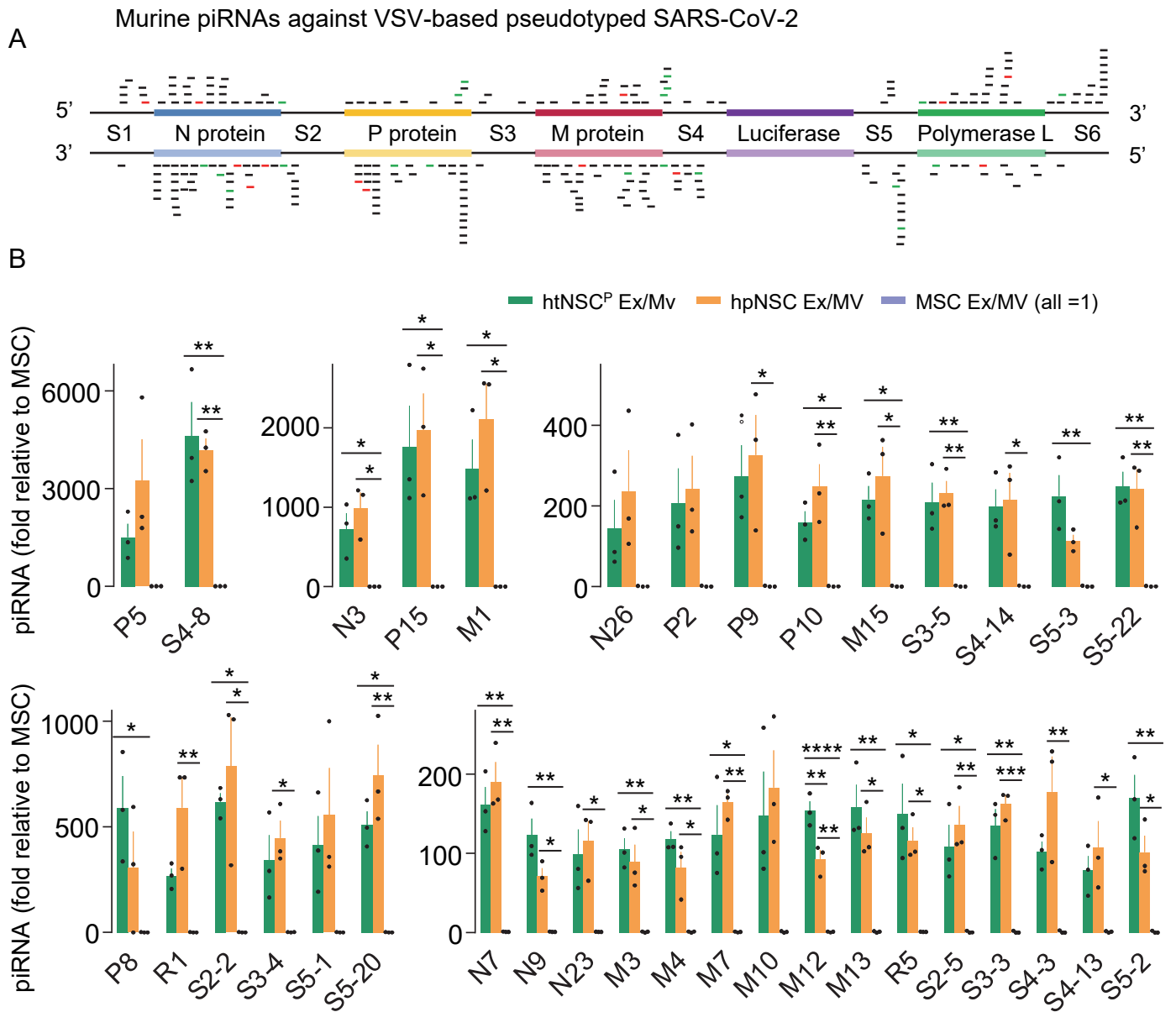


Figure S3

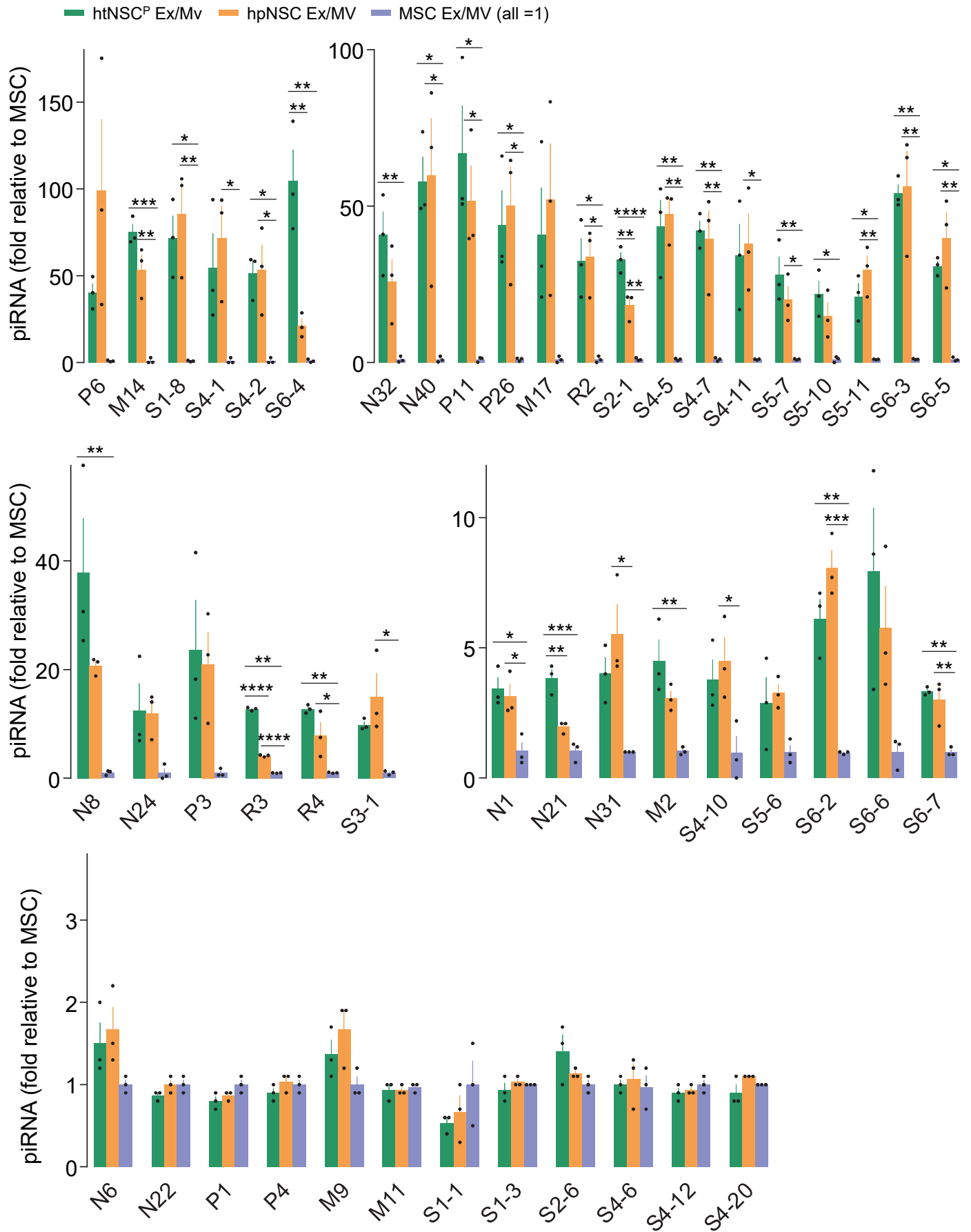


Figure S4

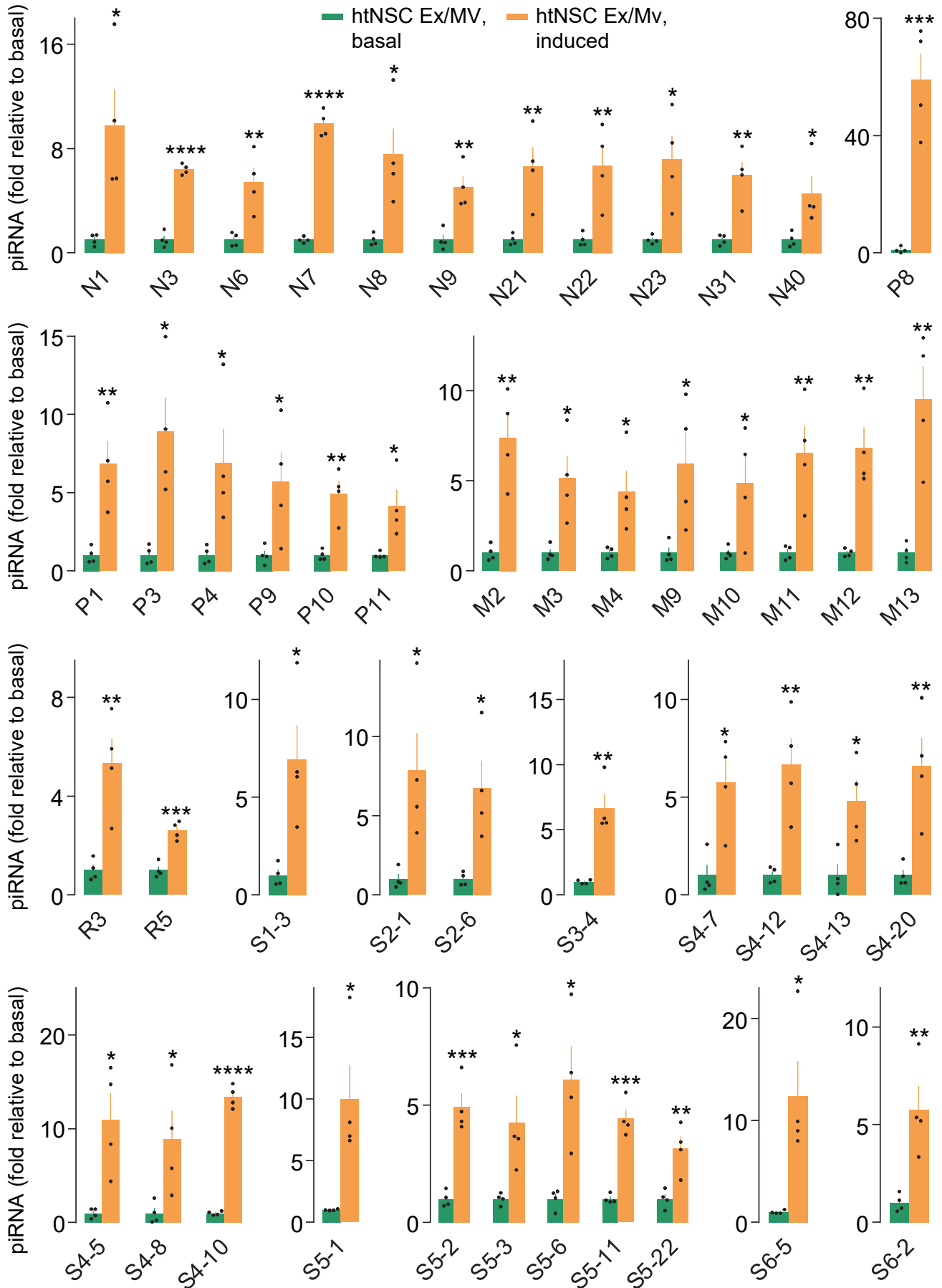


Figure S5

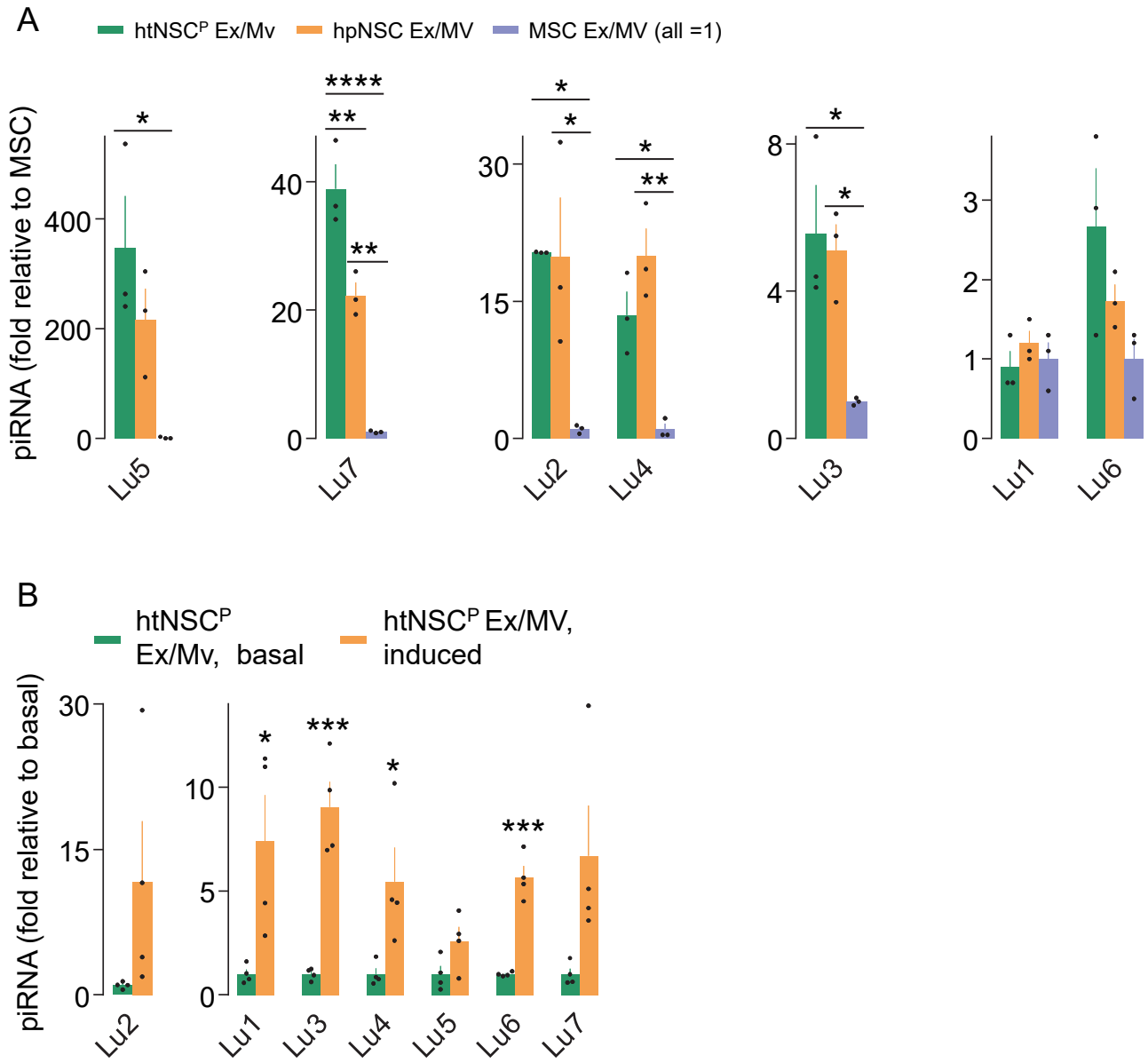


Figure S6

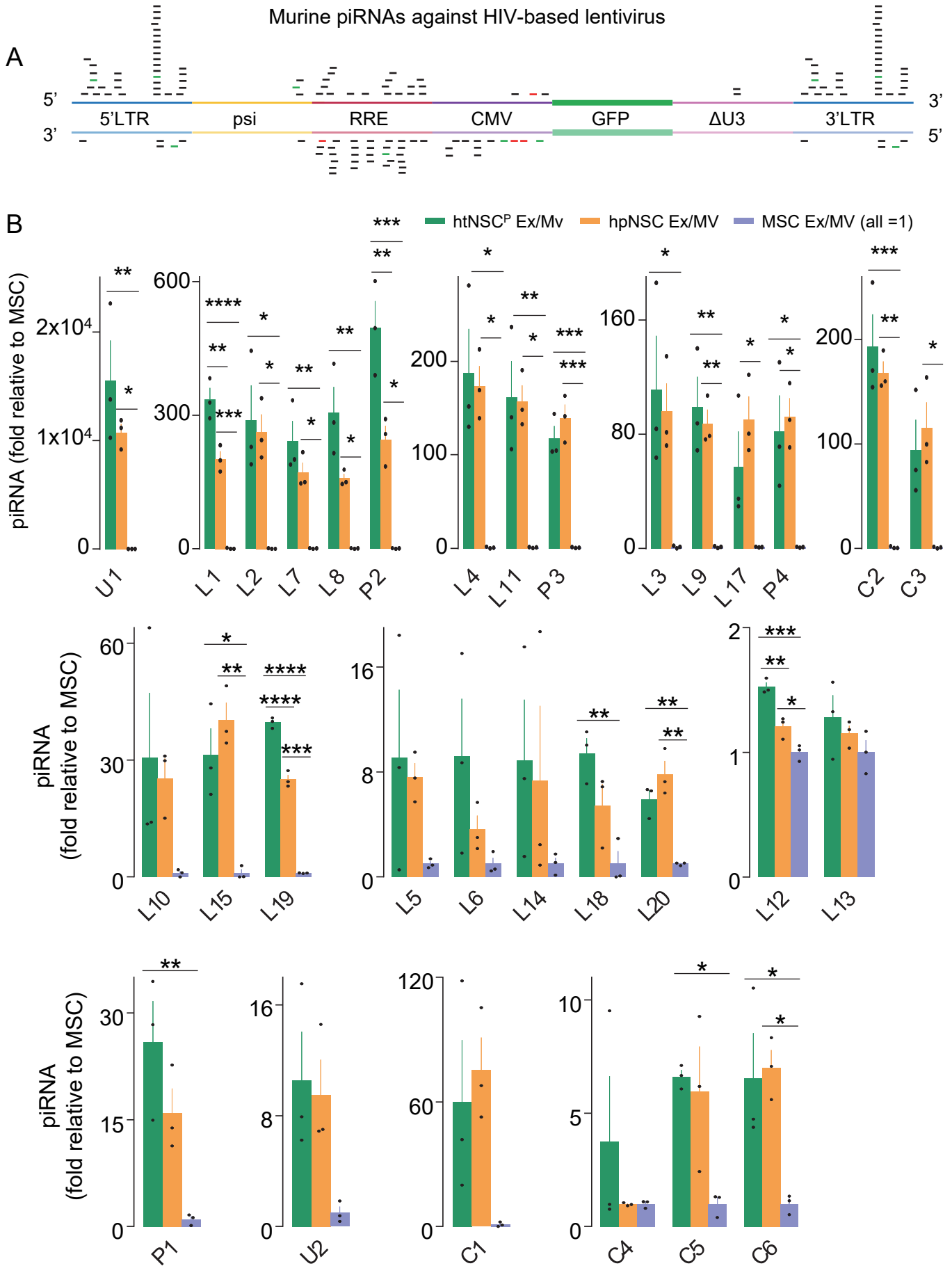


Figure S7

